Combining suspended sediment monitoring and fingerprinting to determine the spatial origin of fine sediment in a mountainous river catchment

O. Evrard, O. Navratil, S. Ayrault, M. Ahmadi, J. Némery, C. Legout, I. Lefèvre, A. Poirel, P. Bonte, M. Esteves

Combining suspended sediment monitoring and fingerprinting to determine the spatial origin of fine sediment in a mountainous river catchment

Olivier Evrard[a], Oldrich Navratil[b,d], Sophie Ayrault[a], Mehdi Ahmadi[a], Julien Némery[b], Cédric Legout[b], Irène Lefèvre[a], Alain Poirel[c], Philippe Bonté[a], Michel Esteves[b]

[a] Laboratoire des Sciences du Climat et de l'Environnement (LSCE/IPSL) – Unité Mixte de Recherche 8212 (CEA, CNRS, UVSQ), 91198-Gif-sur-Yvette Cedex (France)

[b] Laboratoire d'étude des Transferts en Hydrologie et Environnement (LTHE) – Université de Grenoble / Unité Mixte de Recherche 5564 (CNRS, INPG, IRD, UJF), BP 53, 38041-Grenoble Cedex 9 (France)

[c] EDF-DTG, Electricité de France, Grenoble Cedex 9 (France)

Correspondence to: Olivier Evrard (olivier.evrard@lsce.ipsl.fr); Oldrich Navratil (oldrich.navratil@cemagref.fr)

Short title: Spatial origin of sediment in a mountainous river catchment

Keywords: sediment fingerprinting; river; Monte Carlo mixing model; radionuclides; elemental geochemistry; suspended sediment yield; mountain erosion.

Abstract

An excess of fine sediment (grain size < 2 mm) supply to rivers leads to reservoir siltation, water contamination and operational problems for hydroelectric power plants in numerous catchments of the world, such as in the French Alps. These problems are exacerbated in mountainous environments characterised by large sediment exports during very short periods. This study combined river flow records as well as sediment geochemistry and associated radionuclide concentrations as input properties to a Monte Carlo mixing model to quantify the contribution of different geologic sources to river sediment. Overall, between 2007-2009, erosion rates reached 249 ± 75 t km^{-2} yr^{-1} at the outlet of the Bléone catchment, but this mean value masked important spatial variations of erosion intensity within the catchment (85–5000 t km^{-2} yr^{-1}). Quantifying the contribution of different potential sources to river sediment required the application of sediment fingerprinting using a Monte Carlo mixing model. This model allowed the specific contributions of different geological sub-types (i.e., black marls, marly limestones, conglomerates and Quaternary deposits) to be determined. Even though they generate locally very high erosion rates, black marls supplied only a minor fraction (5–20%) of the fine sediment collected on the riverbed in the vicinity of the 907-km^2 catchment outlet. The bulk of sediment was provided by Quaternary deposits (21–66%), conglomerates (3–44%) and limestones (9–27%). Even though bioengineering works conducted currently to stabilise gullies in black marl terrains are undoubtedly useful to limit sediment supply to the Bléone river, erosion generated by other substrate sources dominated between 2007-2009 in this catchment.

1. Introduction

Fine sediment particles (grain-size <2mm) transported in suspension by rivers play an essential role in the environment, because they facilitate significant transfers of carbon and nutrients (House and Warwick, 1999; Collins et al., 2005; Quinton et al., 2010). An excess of suspended sediment in rivers can also lead to numerous problems in downstream areas (Owens et al., 2005). It causes for instance an increase in water turbidity and a rapid filling of reservoirs. Sediment is also associated with numerous contaminants (e.g., metals, organic compounds, antibiotics; e.g. Tamtam et al., 2008; Le Cloarec et al., 2010). These chemicals can desorb from sediment and have the potential to bioaccumulate in organisms such as fishes and lead to public health problems after their consumption (e.g. Sánchez-Chardi, 2009; Urban et al., 2009). In mountainous environments, the problems associated with sedimentation are exacerbated by the fact that the bulk of sediment is exported within very short periods, after violent storms or during the annual snowmelt (e.g., Meybeck et al., 2003). Mano et al. (2009) showed for instance that 40–80% of the annual flux of suspended sediment occurred within 2% of the time in four Alpine catchments (i.e., Asse, Bléone, Ferrand and Romanche catchments). Major erosion events need to be anticipated – e.g. by improving reservoir management – or even controlled in upstream reaches and hillslopes to prevent problems. To meet this objective, sediment source areas first need to be delineated. Furthermore, the relative contribution of these distinct sediment sources to the total sediment export by the river needs to be quantified.

An efficient way to determine the sediment sources within a catchment consists of fingerprinting them. Sediments are indeed influenced by the physical and chemical properties of their source areas. In recent years, a trend to increase the number of potential diagnostic

properties has been observed, by combining properties, for example mineralogy, magnetism and environmental radionuclides. So far, most sediment fingerprinting studies have been applied in the UK (e.g., Collins and Walling, 2002; Walling, 2005) as well as in Australia (e.g., Wasson et al., 2002; Hughes et al., 2009). In France, similar fingerprinting studies have already been carried out, but they were restricted to large river systems such as the Rhône river or the Seine river (e.g. Pont et al., 2002; Tessier and Bonté, 2002; Antonelli et al., 2008). However, to our knowledge, the spatial origin of sediment has not been determined yet at the scale of intermediate mountainous river catchments (500–1000 km^2). In the Alps, several studies have highlighted the important contribution of areas covered by Jurassic black marls to erosion (e.g., Esteves et al., 2005; Mathys et al., 2005; Navratil et al., 2010), as well as the influence of the climate (i.e., Mediterranean vs. mountainous) and the snowmelt on river discharge and suspended sediment concentrations which are characterised by a strong spatial and temporal variability (e.g. Mano et al., 2009). Knowledge regarding the sediment sources in those mountainous areas is nevertheless required to guide the implementation of management measures in order to provide a balanced sediment supply to the river network. The main problem consists in finding appropriate techniques to meet this objective.

On the one hand, the use of traditional river gauging methods has several drawbacks. Typically, discharges and suspended sediment concentrations are only measured at the catchment outlet (e.g., Schmidt and Morche, 2006; Soler et al., 2008; Mano et al., 2009). This method is not able to quantify the erosion processes occurring within the catchment. Furthermore, a spatially-distributed monitoring network is difficult to set up and time-consuming to undertake. Moreover, it can possibly miss important erosion events because of their random occurrence. On the other hand, large catchment-scale erosion modelling studies can offer a solution but they generally need numerous and detailed field data (e.g., soil depth)

which can be difficult to collect at the scale of an entire mountain catchment. Furthermore, the model outputs need to be calibrated and compared to reliable field data for validation.

In this study, we used a combination of flow and sediment concentration monitoring data from six stations distributed across the 907 km^2 Bléone catchment, in the French southern Alps. The Malijai reservoir, located at the outlet of the Bléone catchment (Fig. 1), is being rapidly filled with sediment. The Malijai dam is mainly used to divert water into a canal and to convey it to hydroelectric power plants located downstream along the Durance river (Fig. 1). High suspended sediment loads lead to operational problems for electricity production and to a degradation of water quality (Accornero et al., 2008). To date, much of the erosion mitigation works in the catchment have concentrated on the areas underlain by black marls, which cover 10% of the catchment area. These black marls are considered to be highly erodible (e.g., Rey, 2009). However, to determine the dominant sources of sediment in the entire catchment, we conducted a sediment tracing study during the 2007-2009 period, based on sediment geochemistry and fallout radionuclide concentrations. The implications for future catchment management actions aimed at decreasing the supply of sediment to the reservoir are then discussed.

2. Materials and methods

2.1. Study area

The Bléone catchment (907 km^2; lat.: 44°05'34''N, long.: 06°13'53''E), with altitude ranging between 405 and 2960 m ASL (Above Sea Level), is a mountainous subalpine catchment located in the Durance river district, in southeastern France (Fig. 1a). The catchment is characterised by a dendritic drainage network dominated by the Bléone river and

several tributaries, among which the Bès, the Arigéol, the Duyes, the Bouinenc and the Eaux Chaudes rivers are the most important (Fig. 1b). Most of them are braided rivers with large and well-developed river channels. The climate of the region is transitional and undergoes continental and Mediterranean influences. Mean annual temperature fluctuates between 4–7°C at 585 m ASL (during the 1993-2008 period at Digne-les-Bains; Fig. 1b), with a high temperature range between summer and winter (ca. 18°C). Mean annual rainfall in the catchment varies between 600 and 1200 mm at 400 m ASL. Rainfall is characterised by important seasonal variations, with a maximum in spring and autumn (Mano et al., 2009). Spring and autumn rainfall maxima lead to peak flows in the river. The peak flow observed in spring is accentuated by the snowmelt. In contrast, low base-flow periods are observed in summer and winter. Heavy convective storms mostly occur between June and September, but they affect only local areas. In winter, the low water stage of the river is mostly explained by the predominance of snowfall (Mano et al., 2009).

Severely eroded areas were identified on aerial photographs (with 0.5-m resolution) taken during flight campaigns conducted in 2004, and delineated in a GIS (Arcview, ESRI, Redlands, USA). Digitised 1:50,000 spatially-distributed geological data of the catchment were provided by the French Geological Survey (BRGM). The bedrock is calcareous (marls, conglomerates, limestones), with large exposed areas of Cretaceous and Jurassic black marls, as well as Lias marly limestones (Fig. 2). The areas covered by black marls are severely affected by erosion and they are characterised by a badland morphology (Mathys et al., 2005). Forest is by far the main land use in the catchment (43.6% of the total catchment surface). Urban land (0.7%) is sparse (with the notable exception of the town of Digne-les-Bains; Fig. 1b) and rock outcrops are restricted to limited areas located close to the summits (6.9%). Grassland covers 13.1% of the surface and arable land mostly occupies parts of the river valleys, covering 5.0% of the total catchment surface. The most common crops planted in the

catchment are wheat and corn. In this catchment, erosion is concentrated in areas characterised by a sparse vegetation cover (30.7% of the total catchment surface).

2.2. **Rainfall measurement**

Ten rain-gauges managed by the French *Cemagref* research agency and the *Laboratoire d'étude des Transferts en Hydrologie et Environnement* provided continuous precipitation records. Five meteorological stations managed by the French meteorological office (*Météo France*) provided precipitation depths and durations, snow depth, temperature as well as information on the type of precipitation events (i.e., rain, snow or hail; Fig. 1b). All these stations provided daily records (with the exception of one station providing hourly records; Table 1).

2.3. Hydrological analysis

Six river gauging stations (Table 1) were installed in the catchment (Fig. 1b). An overview of the most relevant parameters describing the location and the area draining to the stations is given in Table 1. This network combined discharge and Suspended Sediment Concentration (*SSC*) monitoring at the outlet of the Bléone catchment, on upstream sections of the headwater rivers (Bès and Upper Bléone) and on three tributaries flowing across areas characterised by different geological bedrocks and land uses (Fig. 2).

Four stations (Robine on the Galabre river; Prads on the Bléone river; Mallemoisson on the Duyes river; and Draix on the Laval torrent) were equipped with a 24-GHz radar (Paratronic Crusoe®) to measure the water level. At the two remaining stations (Pérouré on the Bès river; and Malijai at the outlet of the Bléone catchment), flow discharges were

respectively provided by the *Flood Forecasting Service* (SPC-Grand Delta) and the *Electricité de France* (EDF) company (Poirel, 2004; Mano et al., 2009). Flow discharges were regularly gauged – every month during base-flow and flood events – using 1) the salt (NaCl) dilution method or a current meter for water discharges ≤ 5 m^3 s^{-1} ; and 2) the Rhodamine WT dilution method for floods characterised by a discharge > 5 m^3 s^{-1} and low *SSC* (< 0.01 g L^{-1}). Water level-discharge rating curves were built for each site, which provided discharge estimations with a maximum of 20 % uncertainties (Navratil et al., in review). At all the six stations, a nephelometric turbidimeter (WTW Visolid® 700-IQ and Hach Lange® at Malijai) measured the turbidity using the backscattering of infrared light. These sensors are self-cleaning to prevent a drift in the turbidity records. Furthermore, they can cover a wide range of sediment concentrations (0–300 g L^{-1} SiO_2).

A high frequency sampling strategy was chosen to estimate discharge and *SSC* at each station. Frequency of data acquisition (i.e. water level and turbidity time series) was set up taking account of flow discharge and *SSC* dynamics in each sub-catchment (Table 1). A sequential sampler (Teledyne ISCO 3700) containing 24 one-litre bottles was programmed following the method described by Lewis (1996). This method proposed to trigger the water sampling as soon as critical turbidity thresholds are reached (for details, see Navratil et al., in review). Water and sediment were then sampled at regular intervals which depend on the selected thresholds. These parameters were determined for each station based on local *SSC* dynamics, which depend on seasonal and site-specific characteristics. A data logger recorded the water level and the turbidity and transmitted those data to the laboratory using mobile phones or modems for a daily data quality check.

In the laboratory, *SSC* of each sample was measured using two different methods (AFNOR T90-105, 1994). At low concentrations (< 2 g L^{-1}), a sub-sample of ca. 500 ml was filtered using pre-weighted fibreglass Durieux filters (pore diameter of 0.7 µm), dried for 5

hours at 105°C and then weighed. For concentrations ≥ 2 g L^{-1}, *SSC* was estimated by weighing a subsample of ca. 200 ml after drying it for 24 hours at 105°C. A turbidity-*SSC* calibration curve was built for each station using a polynomial function and this curve was then used to derive the *SSC* time series. Although this relationship was reliable and applicable to most events, turbidity-*SSC* hysteretic relationships were found and considered in a few cases following the methodology proposed by Lewis and Eads (2008). These hysteretic relationships are likely due to variations in sediment size and/or in mineralogy during certain floods (see for similar examples Orwin and Smart, 2004; Downing, 2006). Suspended sediment flux *SSF* [t s^{-1}] was then calculated using Eq. (1).

$$SSF = Q \cdot SSC \cdot 10^{-3} \quad (1)$$

with *Q* corresponding to instantaneous water discharges (m^3 s^{-1}) and *SSC* to instantaneous Suspended Sediment Concentrations (g L^{-1}).

Suspended sediment yield [*SSY* (in ton, t)] was calculated for each flood using Eq. (2):

$$SSY = \int_{t_0}^{t_f} SSF \; dt \quad (2)$$

with t_0 and t_f corresponding to the beginning and the end of the period considered.

Uncertainties associated with *SSC* mainly arose from the use of the turbidity calibration curve, the representativeness of the automatic sediment collection by ISCO samplers (i.e. position of the intake pipe in the water flow and *SSC* homogeneity in the channel cross-section) and laboratory errors (Navratil et al., in review). Uncertainties associated with SSY values reflect cumulated uncertainties for both SSC and discharge. Navratil et al. (in review) showed that uncertainties reached a mean of 20% for *SSC* and 30 % for *SSY* at the Robine station, on the Galabre river. Uncertainties on *SSC* and *SSY* at the other stations were estimated to be of the same order of magnitude as at Robine.

2.4. Soil and riverbed sampling

All soil and riverbed samples were collected with non-metallic trowels in order to avoid sample contamination. Riverbed sediment samples were collected between 2007 and 2009 after the occurrence of widespread rainfall events across the catchment (Table 2). Exposed riverbed sampling sites were selected along the main channels of the river networks, upstream and downstream of the junctions between the trunk river and its tributaries, i.e. at a distance allowing a good homogenization of sediment. Several sub-samples (~ 10) were collected for each location and used to prepare a composite sample representative of the sediment deposited on the river bed at that location. Riverbed sediment was selected as an alternative to suspended sediment in order to increase the spatial coverage of our survey within the catchment.

Representative soil samples (n=150) were also collected to characterise potential source materials. They were mostly taken on colluvial toeslopes adjacent to the drainage network to be representative of material eroded from adjacent hillslopes. Soil samples were dried at 105°C, whereas river bed samples were dried at 40°C to facilitate their grinding. All samples were disaggregated prior to analysis. Sampling sites were systematically located in the field using a portable GPS device (spatial accuracy of 1-5 m) and introduced into a GIS (ArcGIS, ESRI).

2.5. Measurement of radionuclide and elemental geochemistry

All riverbed sediment and soil samples were dried and sieved (< 2 mm) before analysis. Radionuclides were measured in all the collected samples (n=179), whereas the analyses of elemental geochemistry were carried out on a selection of sub-samples (n=80).

For the measurement of radionuclides in each sample, we analysed ~80 g of material. Radionuclide (Am-241, Be-7, Cs-137, excess Pb-210, K-40, Ra-226, Ra-228, Th-228, Th-234) concentrations were determined by gamma-spectrometry using the very low-background coaxial N- and P-types GeHP detectors (Canberra / Ortec) at the *Laboratoire des Sciences du Climat et de l'Environnement* (Gif-sur-Yvette, France). The radionuclide activities were corrected for decay back to the time of sampling.

For the measurement of elemental geochemistry, Rare Earth Elements (REE; i.e. Ce, Eu, La, Lu, Sm, Tb, Yb), three major elements (Fe, K, Na) and several trace elements (As, Ba, Co, Cr, Cs, Hf, Sc, Ta, Th, Zn) were analysed by Instrumental Neutron Activation Analysis (INAA). The uncertainty on these measurements is $\leq 5\%$.

Similar sub-samples were also analysed by Inductively Coupled Plasma – Mass Spectrometry (ICP-MS; XIICCT Series, Thermon Electron), in solutions containing 0.2 g of solid L^{-1}. The total digestion procedure applied to the sediment is described by Le Cloarec et al. (2010). Concentrations were determined for several major (Al, Ca, Mg, Ti) and trace (Ag, Ba, Cd, Cu, Mn, Ni, Pb, Sb, Se, Tl, V) elements. Analytical uncertainties associated with this method did not exceed 10%.

2.6. Selection of fingerprints and design of a mixing model

Based on the French Geological Survey (BRGM) map of the catchment, we grouped the geological classes represented on the map and corresponding to our sediment source samples into seven main sediment source types, i.e. marly limestones, grey marls, conglomerates and sandstones, Quaternary deposits, black marls of Callovo-Oxfordian and Bathonian age (the so-called “Terres Noires”), other black marls and gypsum. Gypsum was excluded from the fingerprinting analysis because of its rapid dissolution in the river (Porta et al., 1998).

Furthermore, to apply the sediment fingerprinting method, we checked that the grain size of soil particles and river sediment was of the same order of magnitude to avoid disturbances due to sorting of particle size that could induce changes in mineralogy and geochemistry of particles. To obtain information on the grain size of sediment, we used the scandium (Sc) concentrations provided by Instrumental Neutron Activation Analysis (INAA; see Section 2.5). Concentration in this trace element is widely used as a proxy of the fine grain size fraction of sediment (e.g., Jin et al., 2006; Dias and Prudêncio, 2008). Non-parametric Wilcoxon tests were then performed to check whether there was a significant grain size difference between soil and sediment samples.

Each potential sediment source class was characterised by its mean concentration/activity and by the standard deviation of each of the 36 fingerprinting properties measured in the samples (Sc was excluded from the list of potential fingerprinting properties, because of its use as a proxy of the fine grain size fraction). The ability of the 36 potential fingerprinting properties to discriminate between the potential sediment sources was investigated by conducting the non-parametric Kruskal-Wallis *H*-test, as initially proposed by Collins and Walling (2002). The Kruskal-Wallis *H*-Test was used as a basis for recognizing and eliminating redundant fingerprint properties. Greater inter-category differences generated larger *H*-test statistics. The null hypothesis stating that measurements of fingerprint properties exhibit no significant differences between source categories was rejected as soon as the *H*-test statistics reached the critical threshold that had been fixed.

Based on the set of discriminating properties retained, an optimum (i.e., the smallest) 'composite fingerprint' was identified by performing a stepwise selection procedure. This second step involved the further testing of properties that successfully passed the first step, using a Stepwise Discriminant Function Analysis (SDFA). As suggested by Collins and Walling (2002), the minimization of Wilk's lambda was used as a stepwise selection

algorithm to identify the set of parameters which, once combined, were able to distinguish correctly and optimally 100% of the source samples. Wilk's lambda is equal to one when all the group means are equal. It approaches zero when the within-group variability is small compared to the total variability. The fingerprinting properties allowing a better discrimination of different sources are hence associated with lower lambda values.

To characterise the properties of each group of sources selected by the Wilk's lambda procedure, we assumed that their concentrations ($c_{i,j}$) could be represented by a normal distribution (Eq. 3).

$$c_{i,j} \approx N(\mu, \sigma^2) \quad (3)$$

where j is a specific group of sources; i is a specific fingerprinting property; μ is the average concentration in fingerprint property i measured in source j; and σ^2 (Eq. 4) is the variance of the probability distribution of the mean of property i in source j (Small et al., 2002).

$$\hat{\sigma}^2 = \left(\frac{S.D.}{\sqrt{d}} \right)^2 \quad (4)$$

where d is the number of independent samples and $S.D.$ is the standard deviation associated with the values of the fingerprinting properties measured in the samples.

A multivariate mixing model was then used to estimate the relative contribution of the potential sediment sources in each riverbed sediment sample (Eq. 5).

$$\begin{bmatrix} \bar{c}_{1,1} & \bar{c}_{1,2} & \dots & \dots & \bar{c}_{1,S} \\ \bar{c}_{2,1} & \bar{c}_{2,2} & \dots & \dots & \bar{c}_{2,S} \\ \dots & \dots & \bar{c}_{i,j} & \dots & \dots \\ \dots & \dots & \dots & \dots & \dots \\ \bar{c}_{V,1} & \dots & \dots & \dots & \bar{c}_{V,S} \end{bmatrix} \begin{bmatrix} \hat{\beta}_1 \\ \dots \\ \hat{\beta}_j \\ \dots \\ \hat{\beta}_S \end{bmatrix} = \begin{bmatrix} y_1 \\ \dots \\ y_j \\ \dots \\ y_V \end{bmatrix} \quad (5)$$

where $\overline{c_{i,j}}$ is the mean value of fingerprinting property i measured in source j ; $\hat{\beta}_j$ is the coefficient representing the contribution of source j to river sediment; S corresponds to the

seven potential sediment sources and *V* represents the fingerprinting properties selected by the Wilk's lambda procedure.

This matrix can be expressed as in Eq. (6):

$$\hat{\beta} = \left(C^{'}C\right)^{-1} C^{'}Y \qquad (6)$$

to which we applied the following physical constraints:

$$\sum_{j=1}^{S} \hat{\beta}_j = 1; \quad 0 \le \hat{\beta}_j \le 1 \qquad (7)$$

The constraints of Eq. (7) ensured that the sum of all source contributions in the riverbed sediment was equal to one and that each fraction of these contributions was between zero and one, inclusive.

A significant uncertainty exists in the estimation of $\bar{c}_{i,j}$ (average of all concentrations *c* in a specific sediment source) because we could only collect a limited number of samples in the field. Therefore, for modelling this uncertainty and for incorporating its effects into the mixing model, we used the variance of the distribution as proposed by Small et al. (2002) (Eq. 4). Based on the Monte Carlo method, a series of p=10,000 random positive numbers was then generated for each fingerprinting property and for each source. The robustness of the source ascription solutions β_j was then assessed using a mean 'goodness of fit' (*GOF*) index (Eq. 8; Motha et al., 2003).

$$GOF = 1 - \left\{ \frac{1}{p} \times \left(\sum_{i=1}^{V} \frac{\left| y_i - \sum_{j=1}^{S} \hat{\beta}_j \bar{c}_{i,j} \right|}{y_i} \right) \right\} \qquad (8)$$

We only used the sets of simulated random numbers that obtained a *GOF* index value higher than 0.80 in the subsequent steps. This threshold was fixed using a binomial case of goodness of fit with a degree of freedom equal to the number of sources minus 1, and referring to the Chi-square distribution table. The use of the Monte Carlo method allowed the calculation of 95-% confidence intervals.

2.7.Coupling the sediment fingerprint approach and suspended sediment monitoring

Surface percentages of severely eroded areas located on each geological substrate type (Table 1) and draining to each monitoring station were estimated by GIS analysis. They were used to estimate the total *SSY* proportion associated with each geologic type. We hypothesised that eroded areas delineated on aerial photographs contributed proportionally to their area to the suspended sediment yields, whatever their geologic type. Then, we compared those eroded area fractions (hereafter referred to as EA%) to the results provided by the fingerprinting mixing model (hereafter referred to as MM%) for the riverbed samples located in the vicinity of all monitoring stations, except one (*SSY* data were missing for the station located along the Laval torrent at Draix). We hypothesised that the comparison of both approaches would outline the contrasted erodibility of the different geological substrates.

Erosion rates were estimated for each substrate type and each monitored sub-catchment. To this end, we based our calculations on mean inter-annual *SSY*-values estimated during the 2007-2009 period (Figure 3). We hypothesised that the composition of riverbed samples collected close to the monitoring stations was representative of the sediment composition in the river at this location over several years, given it was systematically collected after widespread rainfall events throughout the catchment (Table 2). However, it is probably more reasonable to postulate that MM% mostly depends on the characteristics of the most important flood that occurred before our sampling. We therefore calculated the *SSY* (at both annual and flood scales) associated with each geologic substrate type using the sediment type composition estimated by the mixing model (MM%). This SSY fraction was then normalised to the surface of severely eroded areas belonging to each geologic substrate type and normalised to the duration of the period considered, i.e. two years for the calculations

conducted over the 2007-2009 period, but only several hours (i.e., depending on the duration of the sedigraph) for the calculations conducted at the flood scale.

3. Results

3.1. Sediment yields

The analysis of aerial photographs outlined 2126 eroded areas in the catchment. Their surface was highly variable (between 811 m^2 and 1.85 km^2, with a mean surface of 45,000 m^2). They were classified into three groups, i.e. mass movement areas (22 % of the total eroded area), sheet and rill erosion areas (48%), and gully erosion areas (30%).

The monitored hydrological years (i.e. Oct. 2007- Sept. 2008 and Oct. 2008 – Sept. 2009) were rather wet (i.e. 1045 mm and 953 mm, respectively) when compared to the mean annual rainfall depth recorded from 1934 to 2009, i.e. 820 mm yr^{-1} (data for the Seyne raingauge; *Météo France*). Rainfall increased with altitude (710 mm at 690 m ASL – data for the Marcoux raingauge; 1000 mm at 1350 m ASL – data for the Seyne raingauge) and was then strongly heterogeneous within the catchment, depending on the dominant weather system. On average, a runoff depth of ca. 400 mm yr^{-1} was measured at the monitoring stations (Table 3), and this value appeared to remain rather stable from one station to another (i.e. coefficient of variation of 26% in 2007-2009). However, the Galabre and the Duyes sub-catchments displayed the lowest mean annual runoff coefficient (30%), compared to the runoff coefficients calculated for the other sub-catchments (between 44-62%). Overall, runoff remained relatively constant during the two monitored years, probably because of equivalent rainfall inputs (mean variation of 11%). However, a strong inter-annual runoff variation was specifically observed on the Duyes river, at Mallemoisson, with 545 mm runoff in 2007-2008, but only 139 mm in 2008-2009. This low runoff value can be attributed to the non-occurrence

of widespread rainfall events in this sub-catchment in 2008-2009. Furthermore, very few storms affected this sub-catchment. They rather occurred in upstream parts of the catchment (i.e. in the Upper Bès and Upper Bléone sub-catchments).

Maximum discharges observed during the 2007-2009 period corresponded to floods with 1-year return periods (according to local data available for the Bès river at Pérouré for the 1963-2009 period; *SPC-Grand Delta*). We can therefore confidently say that no widespread extreme flood occurred in the catchment during those two years.

SSY measured at the Bléone catchment outlet between October 2007 and September 2009 was 432,400 ± 130,000 tons (Table 3; Figure 3). This value corresponds to a specific sediment yield (*SSY**) of 249 ± 75 t km^{-2} yr^{-1}. However, *SSY** were very variable within the Bléone catchment (Figure 3). They varied between 85 ± 25 t km^{-2} yr^{-1} on the Duyes river at Mallemoisson and 5000 ± 1500 t km^{-2} yr^{-1} on the Laval torrent at Draix. These rates are of the same order of magnitude as those observed in other catchments of the French Southern Alps or in other similar mountainous contexts (e.g. Mathys et al., 2003; López-Tarazón et al., 2009). These *SSY** were correlated (R^2 = 0.62) with the proportion of the sub-catchment covered by marls (5% in Les Duyes vs. 94% upstream of Laval). Overall, *SSY* measured in all sub-catchments in 2007-2008 (e.g. 431 ± 130 t km^{-2} yr^{-1} at the catchment outlet) were higher than the rates measured in 2008-2009 (e.g. 65 ± 20 t km^{-2} yr^{-1} at the outlet), even though the total precipitation depths remained equivalent during both hydrological years (Figure 3). This difference in sediment yields can partly be explained by the presence of a deep and persistent snow cover during the 2009 winter and spring seasons, which probably protected the soil against erosion. In 2008-2009, 206 days of snow were recorded at 1300 m ASL (with a complete snowmelt on March 30, 2009), vs. only 136 days in 2007-2008 (with a complete snowmelt on February 15, 2008). Moreover, in 2007-2008, the bulk of the sediment yield was mainly attributed to south-western Mediterranean events, whereas in 2008-2009, convective

storms dominated. In 2007-2008, storms produced for instance 24% of erosion recorded in the Bès river at Pérouré (vs. 76% of erosion generated by Mediterranean events). In contrast, in 2008-2009, convective storms produced 66% of the annual SSY at the same station. Those storms generated high SSY in small sub-catchments (e.g. Laval), but the bulk of this sediment probably deposited along the river network, between upstream sub-catchments and the catchment outlet.

3.2. Radionuclide analysis

In total, 179 soil surface and sediment samples were analysed by gamma-spectrometry (Fig. 4). Cs-137 and excess Pb-210 activities were the highest close to the summits (70.7 Bq kg^{-1} ± 57.1 for Cs-137; 49.9 Bq kg^{-1} ± 28.8 for excess Pb-210), as well is in the sub-catchment of the Duyes river (65 Bq kg^{-1} ± 44.8 for Cs-137 in all the samples collected in this sub-catchment; 33.3 Bq kg^{-1} ± 19.5 for excess Pb-210; Table 4). In contrast, activities of those radionuclides were much lower close to the outlet (2.0 ± 1.5 for Cs-137; 1.6 Bq kg^{-1} ± 3.7 for excess Pb-210; Table 4). Activities of Cs-137 and excess Pb-210 were well correlated (R^2 = 0.68) across the catchment and they displayed similar spatial patterns. The Cs-137/ Be-7 ratio allowed highlighting the dominant erosion processes occurring in the different sub-catchments (e.g., Olley et al., 1993). As already mentioned above, Cs-137, which has a half-life of 30 years, was supplied to the atmosphere by testing of nuclear weapons and by the catastrophe of Chernobyl. Cs-137 activities in soils therefore decrease by natural decay and by the transfer of fine sediment to rivers. In contrast, Be-7 is a cosmogenic radionuclide that is continuously supplied to soils by rainfall. It is characterised by a short half-life period (53 days).

Eroded soils in the Upper Bléone and the Upper Bès sub-catchments were characterised by high activities in both Cs-137 and Be-7, which indicates that those upstream areas were mostly affected by sheet erosion (i.e. erosion generated by overland flow; Cerdan et al., 2006) of surface soils enriched in Cs-137. In contrast, areas characterised by a high Cs-137 content and low Be-7 concentrations are rather dominated by rill erosion (i.e. forming several-cm depth channels; Cerdan et al., 2006). Most soil eroded from the Lower Bès and the Galabre sub-catchments typically fell within this category. In the areas characterised by a low Cs-137 and a high Be-7 content (e.g. in parts of the Galabre and the Chanolette sub-catchments), gully erosion was the major process. When Cs-137 and Be-7 concentrations were relatively low and equivalent, the bulk of erosion occurred as gully collapse, which was observed in the Eaux Chaudes sub-catchment.

3.3. Geochemical analysis

Table 5 shows the radionuclide activities and the concentrations in major and trace elements measured in soil samples representative of the seven dominant geological substrate types observed in the catchment, and Table 6 provides similar information for the collected riverbed samples. Spatial distribution of the soil concentration in elements (i.e., As, Ba, Br, Co, Cs, Fe, Hf, K, Na, Lu, Rb, Sb, Ta, Tb, Yb, Zn) was asymmetrical (Table 5). Furthermore, when moving along the Bès river from the headwaters up to the junction with the Bléone river (Table 6), the concentrations in riverbed sediment decreased for several elements (As, Fe, Zn, Cu, Pb). In contrast, a clear increase in concentrations was observed in the case of K, Ca and Mg. When moving along the Bès river from the headwaters up to the junction with the Bléone river, the concentrations in riverbed sediment decreased for several elements (As, Fe, Zn, Cu, Pb). In contrast, a clear increase in concentrations was observed in the case of K, Ca and Mg.

3.4. Selection of fingerprinting properties and mixing model

Firstly, we could not detect any significant difference (p = 0.05) of particle size between soil and sediment samples by comparing their scandium concentrations (i.e., 9.9 ± 2.9 mg kg^{-1} for soils vs 7.6 ± 2.9 mg kg^{-1} for river sediment). Among the different potential sediment sources, the Quaternary deposits had the lowest Sc concentration, but it was not significantly different from the concentrations of all the other potential sources.

Results of the Kruskal-Wallis H-test outlined 21 potential variables to discriminate the sediment sources (difference significant at p=0.05; Table 7): Ag, Al, Ba, Co, Cu, Eu, Fe, Hf, La, Lu, Mn, Na, Ni, Ra-226, Rb, Sb, Sm, Ti, Tl, V, Zn. Among those potential variables, 6 properties were sufficient to design the optimum composite fingerprint (Table 8). Only one lithogenic radionuclide was selected (Ra-226). The other selected fingerprints were metals (Al, Ni, V, Cu, Ag).

In total, 10,000 random source concentrations were generated by the Monte Carlo mixing model for each riverbed sediment sample. The outputs of the mixing model appeared to be very stable, all outputs being very close (and systematically within a range of ± 2%) to their mean value. We therefore decided to present only those mean values in the remainder of the text as well as in Figure 5.

The mixing model provided some important information on the sediment sources in the Bléone catchment during the four sampling periods. First, it outlined the important contribution of the local sediment sources to the river. For instance, when moving along the Bès river from the headwaters up to its junction with the Bléone river, the supply of black marls to the riverbed sediment strongly increased (from 15% to 47% when moving on from BE1 > BE 2; Fig. 5a). Further downstream, the increase in geological heterogeneity was

reflected by the multiplicity of sources found along this section (i.e., additional sediment supply by limestones, conglomerates and sandstones). We outlined for instance at location BE7 the additional presence of a fraction of sediment generated by local Quaternary deposits (27%; Fig. 2). A similar behaviour (i.e., the important contribution of local sources to river sediment) was determined by the mixing model along the Bléone river (Fig. 5b; from BL1 to BL11).

Secondly, the mixing model showed that the different tributaries substantially affected the composition of the riverbed sediment collected after the river junctions. For instance, the supply of sediment generated by black marls was particularly evident from the Bouinenc river (increasing from 0 to 42% when moving from BL8 to BL9; Fig. 5b).

Third, certain samples have a rather surprising composition. This was particularly the case of sample BL10, collected after the Bès-Bléone junction (Fig. 5d). It is very likely that this sample was taken at an insufficient distance from the river junction, at several places where a good mixing of all sediment sources was not achieved yet.

Fourth, the contribution of the different sources to riverbed sediment collected close to the outlet seems to vary throughout time (from BL11 to BL13; Fig. 5b-c). In November 2007, conglomerates and Quaternary deposits dominated (Fig. 5b), whereas Quaternary deposits and (marly) limestones provided the bulk of sediment in April 2009 (Fig. 5c).

3.5. Coupling sediment fingerprinting and suspended sediment monitoring

Results of the mixing model (MM%) and fractions of *SSY* (corresponding to the fractions of eroded area, EA%) derived for each individual geological substrate type showed rather different trends (Figure 6 a, b). except for the Bléone river at Malijai, where similar results were obtained when following both approaches. Riverbed sediment at that location

was composed of a mix of the different rock types, with a dominance of conglomerates and Quaternary deposits.

Overall, the estimation of the contribution of limestones/marls to the river sediment was often higher when using the monitoring-based approach compared to the fingerprinting approach (Figure 6a). In contrast, the contribution of black marls, Quaternary deposits and conglomerates to river sediment was generally underestimated by the monitoring approach. This almost general observation probably reflected the different erodibility of the different geological substrate sources.

Erosion rates in severely eroded areas reached on average 3,900 ± 1,200 t km^{-2} yr^{-1} when considering all the rock types observed in the catchment (Figure 7a). However, this average value masks important spatial variations, erosion rates fluctuating between 2,300 ± 700 t km^{-2} yr^{-1} on the Bès river at Pérouré and 6,300 ± 1,900 t km^{-2} yr^{-1} on the Bléone river at Prads. In the area draining to the Laval monitoring station, which is almost exclusively composed of black marls (94% of its surface), erosion rate was estimated at 7,700 ± 2,300 t km^{-2} yr^{-1} according to monitoring during the 2007-2009 period.

When considering erosion rates per rock type (Figure 7a), they fluctuated between 700 ± 200 t km^{-2} yr^{-1} for limestone/marls and 3,500 ± 1,000 t km^{-2} yr^{-1} for Quaternary deposits. Erosion rates can also be expressed in terms of sediment ablation from severely eroded areas (in mm yr^{-1}; Table 9); the density of compacted sediment was used as a first approximation (i.e., 2,650 kg m^{-3}). Quaternary deposits and black marls had similar values (mean of 1.3 – 1.2 mm yr^{-1}, respectively). Conglomerates were associated with a lower value (0.6 mm yr^{-1}). Limestones/marls were characterised by the lowest erosion rate (0.3 mm yr^{-1}). When we restricted this analysis to the major flood that occurred before the riverbed sediment sampling, we observed a much lower variability of the contribution of the different rock types to erosion (Figure 7b): erosion rates fluctuated between a mean value of 1 ± 0.3 t km^{-2} hr^{-1} for

limestones/marls and a mean of 6.5 ± 2 t km^{-2} hr^{-1} for Quaternary deposits. We have to point out that erosion rates estimated for these floods (in t km^{-2} hr^{-1}) appeared to be independent from rainfall volumes and intensities (Figure 7c). Geological substrate type properties (e.g., sensitivity to erosion) explained thus most of erosion rate variations.

4. Discussion

4.1. Erosion processes within the catchment and river management

Calculation of radionuclide ratios (i.e., Cs-137 /Be-7) in soil samples collected in the different sub-catchments outlined the strong diversity of erosion processes occurring in the catchment. The mixing model results also pointed out the important contribution of Quaternary deposits (i.e., mostly glacial sediment, moraines and molasse) and the associated mass movements to the catchment sediment yield. Those deposits cover 27% of the entire sediment surface, but they generated 21% to 66% of the sediment collected on the riverbed close to the outlet. In contrast, even though they produce locally huge sediment quantities, black marls, which cover 10% of the total catchment surface, generated a similar proportion (i.e., 5%–20%) of the sediment collected on the riverbed close to the outlet. If these results are confirmed by further analyses conducted on suspended sediment collected during floods, this finding could have important management implications. Because of locally very high erosion rates in terrains covered by black marls, erosion mitigation was concentrated in those areas (e.g., Rey, 2009). However, at the entire catchment scale, the supply of Quaternary deposits and conglomerates to the river is far from negligible, which probably limits the overall efficiency of the measures implemented.

4.2. Advantages and drawbacks of this coupled approach

Overall, compared to previous sediment fingerprinting studies, the Bléone catchment is geologically very homogeneous, given all its rocks are sedimentary. In contrast, most previous studies conducted in Luxembourg (Martínez-Carreras et al., 2010), in Zambia and in England (Collins and Walling, 2002) as well as in Australia (Hughes et al., 2009) aimed to determine the sediment sources in more heterogeneous areas, composed of a combination of sedimentary and igneous/metamorphic rocks. Nevertheless, the geological homogeneity of the Bléone catchment masks strong local heterogeneities (e.g., local dominance of black marls).

Coupling sediment fingerprinting and suspended sediment monitoring improved our understanding of sediment sources and erosion rates in the Bléone mountainous catchment. However, two main limitations can be pointed out at this stage. First, even though the composition of riverbed samples was found to be rather representative of the source spatial distribution, the composition of certain riverbed sediment samples remained unexplained. It probably also depends on very local factors such as the good mixing conditions of sediment at the sampling point and the local hydraulic conditions prevailing during the flood recession that favoured the sedimentation of the coarser sediment fraction. Even though we aggregated riverbed sediment sampled at different locations and collected them at a reasonable distance from the river junctions, we probably collected the coarser grain-size fraction only. Results of this first approach could then be usefully compared to the fingerprinting of suspended sediment collected during floods in order to take account of the entire grain size distribution, from wash load to fine sands.

Furthermore, in mountainous environments, additional factors control the composition of riverbed sediment: (1) spatial and temporal rainfall patterns, (2) the sediment source heterogeneity, their connectivity to the river network and their distance from the outlet; (3) the temporal variability of the soil cover by snow and vegetation; and (4) the sediment sorting and the abrasion dynamics of the coarser sediment fraction along the river network. For

instance, a sediment sample collected after a heavy and local thunderstorm will probably have a different geochemical composition than the one collected after widespread low-intensity rainfall. Temporary fine sediment storage along the river network will also alter the representativeness of fine sediment collected downstream. Results would probably be slightly or moderately different if they were integrated over longer time periods. This "memory effect" will be particularly important in large river catchments characterised by large braided river patterns and a significant storage capacity of fine sediment (Navratil et al., 2010). This process can explain why, among all our study sites, EA% and MM% were the most similar at the catchment outlet (907 km^2; Figure 6b).

Finally, this study outlines the necessity to take account of several issues associated with the sample representativeness. Spatial variability and evolution of the sediment source contributions along the river network is undeniable. However, our results show the importance of the temporal variability of the sediment source contributions (Fig. 5). Considering the temporal variability of the sediment source contributions by coupling fingerprinting and monitoring approaches (i.e., rainfall, discharge and SSC) with a high sampling frequency could then usefully further improve our understanding of erosion processes occurring in mountainous basins.

5. Conclusions

This study, conducted in a 907-km^2 mountainous catchment of the southern French Alps, is one of the first attempts to combine the use of a continuous river monitoring network and sediment fingerprinting based on radionuclide and elemental geochemistry properties to determine the spatial sources of sediment. Our results showed the strong diversity of the erosion processes observed within the catchment. Erosion rates reached a mean value of 249 ± 75 t km^{-2} yr^{-1} at the outlet of the Bléone catchment, but they greatly fluctuated between the

different sub-catchments (85–5000 t km^{-2} yr^{-1}) mostly because of the occurrence of local heavy storms and the differences of soil erosion intensity. We also outlined the much higher contribution of Quaternary deposits (21–66%), limestones (9–27%) and conglomerates (3–44%) to the river sediment collected at the catchment outlet than the supply of black marls (5–20% at the outlet), which still generated particularly high erosion rates locally. In future, temporal variability of sediment sources within mountainous catchments generated by different weather and flood types should be investigated with a high sampling frequency in order to validate the relevance of those results throughout time. Furthermore, a similar study using suspended sediment instead of riverbed sediment should be conducted to confirm those results.

Acknowledgements

This is the LSCE contribution no. X. This work was part of the STREAMS (*Sediment TRansport and Erosion Across Mountains*) project, funded by the French National Research Agency (ANR/ BLAN06-1_139157). The authors would like to thank Marion Stabholz for her help for preparation and analysis of suspended sediment by ICP-MS and INAA. They also gratefully acknowledge Fred Malinur and Lucas Muller for their help in river monitoring, as well as Nicolle Mathys and Sébastien Klotz (Cemagref) for providing data collected by the Draix Research Observatory and for their useful comments on a draft version of the paper.

References

Accornero A, Gnerre R, Manfra L. 2008. Sediment concentrations of trace metals in the Berre lagoon (France): an assessment of contamination. *Archives of Environmental Contamination and Toxicology,* **54**: 372–385.

630 Antonelli C., Eyrolle F., Rolland B., Provansal M., Sabatier F., 2008. Suspended
631 sediment and ^{137}Cs fluxes during the exceptional December 2003 flood in the Rhone River,
632 southeast France. *Geomorphology*, **95**: 350–360
633 Cerdan, O., Poesen, J., Govers, G., Saby, N., Le Bissonnais, Y., Gobin, A., Vacca, A.,
634 Quinton, J., Auerswald, K., Klik, A., Kwaad, F.P.M., Roxo, M.J., 2006. Sheet and rill
635 erosion. In: Boardman, J., Poesen, J. (Eds). Soil Erosion in Europe. Wiley, Chichester, pp.
636 501-513.
637 Collins, A., Walling, D., 2002. Selecting fingerprint properties for discriminating
638 potential suspended sediment sources in river basins. *Journal of Hydrology*, **261**: 218-244.
639 Collins, A.L., Walling, D.E., Leeks, G.J.L., 2005. Storage of fine-grained sediment and
640 associated contaminants within the channels of lowland permeable catchments in the UK. In
641 *Sediment Budgets 1*, Walling DE, Horowitz A (eds). IAHS Publication No. 291. IAHS
642 Press, Wallingford: 259–268.
643 Dias, M.I., Prudêncio, M.I., 2008. On the importance of using scandium to normalize
644 geochemical data preceding multivariate analyses applied to archaeometric pottery studies.
645 *Microchemical Journal*, **88**, 136-141.
646 Downing, J., 2006. Twenty-five years with OBS sensors: The good, the bad, and the ugly.
647 *Continental Shelf Research*, **26** (17-18): 2299-2318.
648 Esteves, M., Descroix, L., Mathys, N., Lapetite, J., 2005. Field measurement of soil hydraulic
649 properties in a marly gully catchment (Draix, France). *Catena*, **63** (2-3): 282-298.
650 House, W.A., Warwick, M,S., 1999. Interactions of phosphorus with sediments in the River
651 Swale, Yorkshire, UK. *Hydrological Processes*, **13**: 1103–1115.
652 Hughes, A. O., Olley, J.M., Croke, J. C., McKergow, L. A., 2009. Sediment source changes
653 over the last 250 years in a dry-tropical catchment, central Queensland, Australia.
654 *Geomorphology*, **104** (3-4): 262-275.

Jin, Z., Li, F., Cao, J., Wang, S., Yu, J., 2006. Geochemistry of Daihai Lake sediments, Inner Mongolia, north China: implications for provenance, sedimentary sorting, and catchment weathering. *Geomorphology*, **80**, 147-163.

Le Cloarec, M.F., Bonté, P.H., Lestel, L., Lefèvre, I., Ayrault, S., 2010. Sedimentary record of metal contamination in the Seine River during the last century. *Physics and Chemistry of the Earth, Parts A/B/C*. doi:10.1016/j.pce.2009.02.003

Lewis, J., 1996. Turbidity-controlled suspended sediment sampling for runoff-event load estimation. *Water Resources Research*, **32**(7): 2299–2310.

Lewis, J. and Eads, R., 2008. Implementation guide for turbidity threshold sampling: principles, procedures, and analysis. Gen. Tech. Rep. PSW-GTR-212. Albany, CA: U.S. Department of Agriculture, Forest Service, Pacific Southwest Research Station, 86 p.

López-Tarazón, J.A., Batalla, R.J., Vericat, D., Francke, T., 2009. Suspended sediment transport in a highly erodible catchment: The River Isábena (Southern Pyrenees). *Geomorphology*, **109**: 210–221.

Mano, V., Nemery, J., Belleudy, P., Poirel, A., 2009. Assessment of suspended sediment transport in four Alpine watersheds (France): influence of the climatic regime. *Hydrological Processes*, **23:** 777-792.

Martínez-Carreras, N., Krein, A., Gallart, F., Iffly, J.F., Pfister, L., Hoffmann, L., Owens, P.N., 2010. Assessment of different colour parameters for discriminating potential suspended sediment sources and provenance: A multi-scale study in Luxembourg. *Geomorphology*, **118** (1-2), 118-129.

Mathys, N., Brochot, S., Meunier, M., Richard, D., 2003. Erosion quantification in the small marly experimental catchments of Draix (Alpes de Haute Provence, France). Calibration of the ETC rainfall–runoff–erosion model. Catena, **50**: 527– 548

Mathys, N., Klotz, S., Esteves, M., Descroix, L., Lapetite, J., 2005. Runoff and erosion in the Black Marls of the French Alps: Observations and measurements at the plot scale. *Catena*, **63** (2-3): 261-281.

Meybeck, M., Laroche, L., Dürr, H.H., Syvitski, J.P.M., 2003. Global variability of daily total suspended solids and their fluxes in rivers. *Global & Planetary Change*, **39**: 65–93.

Motha, J.A., Wallbrink, P.J., Hairsine, P.B., Grayson, R.B., 2003. Determining the sources of suspended sediment in a forested catchment in southeastern Australia. *Water Resources Research*, **39**: 1059.

Navratil, O., Legout, C., Gateuille, D., Esteves, M., Liebault, F., 2010. Assessment of intermediate fine sediment storage in a braided river reach (Southern French Prealps), *Hydrological Processes,* **24** (10): 1318-1332.

Navratil O., Esteves M., Legout C., Gratiot N., Willmore S., Nemery J., Grangeon T., *in review*. Scaling suspended sediment monitoring uncertainties in a highly erodible mountainous catchment, *Hydrological Processes.*

Olley, J.M., Murray, A.S., Mackenzie, D.H., Edwards, K., 1993. Identifying sediment sources in a gullied catchment using natural and anthropogenic radioactivity. *Water Resources Research*, **29**(4): 1037-1043.

Orwin, J.F., Smart, C.C., 2004. Short-term spatial and temporal patterns of suspended sediment transfer in proglacial channels, Small River Glacier, Canada. *Hydrological Processes*, **18**: 1521-1542.

Owens, P.N., Batalla, R.J., Collins, A.J., Gomez, B., Hicks, D.M., Horowitz, A.J., Kondolf, G.M., Marden, M., Page, M.J., Peacock, D.H., Petticrew, E.L., Salomons, W., Trustrum, N.A., 2005. Fine-grained sediment in river systems: Environmental significance and management issues. *River Research & Applications* **21**: 693-717.

Poirel, A. 2004. Etude du transport solide dans la Durance; Résultats des mesures 2001-2003. EDF internal report, 34 pages.

Pont, D., Simonnet, J.P., Walter, A.V., 2002. Medium-term changes in suspended sediment delivery to the ocean: consequences of catchment heterogeneity and river management (Rhone river, France). *Estuarine, Coastal & Shelf Science*, **54**: 1-18.

Porta, J., 1998. Methodologies for the analysis and characterization of gypsum in soils: A review. *Geoderma*, **87**, 31-46.

Quinton, J., Govers, G., Van Oost, K., Bardgett, R.D., 2010. The impact of agricultural soil erosion on biogeochemical cycling. *Nature Geoscience*, **3**: 311-314.

Rey, F., 2009. A strategy for fine sediment retention with bioengineering works in eroded marly catchments in a mountainous Mediterranean climate (Southern Alps, France). *Land Degradation & Development*, **20**: 210 – 216.

Sánchez-Chardi, A., Oliveira Ribeiro, C. A., Nadal, J., 2009. Metals in liver and kidneys and the effects of chronic exposure to pyrite mine pollution in the shrew *Crocidura russula* inhabiting the protected wetland of Doñana. *Chemosphere*. **76**(3): 387-394.

Schmidt, K. H., Morche, D., 2006. Sediment output and effective discharge in two small high mountain catchments in the Bavarian Alps, Germany. *Geomorphology*, **80** (1-2): 131-145.

Small, I.F., Rowan J.S., Franks, S.W., 2002. Quantitative sediment fingerprinting using a Bayesian uncertainty estimation framework. In: Dyer, F.J., Thoms, M.C., Olley, J.M. (Ed): *The Structure, Function and Management Implications of Fluvial Sedimentary Systems*. Proceedings of an international symposium, Alice Springs (Australia), 2-6 September. IAHS Publication no. 276, pp. 443-450.

Soler, M., Latron, J., Gallart, F., 2008. Relationships between suspended sediment concentrations and discharge in two small research basins in a mountainous Mediterranean area (Vallcebre, Eastern Pyrenees). *Geomorphology*, **98** (1-2), 143-152.

Tessier, L., Bonté, P., 2002. Suspended Sediment Transfer in Seine River Watershed, France: a Strategy Using Fingerprinting From Trace Elements. Conference proceedings for the Science for Water Policy: the implications of the Water Framework Directive, September 2002, 79-99.

Tamtam, F., Mercier, F., Le Bot, B., Eurin, J., Tuc Dinh, Q., Clément, M., Chevreuil, M., 2008. Occurrence and fate of antibiotics in the Seine River in various hydrological conditions. *Science of The Total Environment*, **393** (1): 84-95.

Urban, J.D., Tachovsky, J.A., Haws, L.C., Wikoff Staskal, D., Harris, M.A., 2009. Assessment of human health risks posed by consumption of fish from the Lower Passaic River, New Jersey. *Science of the Total Environment*, **408** (2): 209-224.

Walling, D., 2005. Tracing suspended sediment sources in catchments and river systems. *Science of the Total Environment*, **344**: 159-184.

Wasson, R., Caitcheon, G., Murray, A., McCulloch, M., Quade, J., 2002. Sourcing sediment using multiple tracers in the catchment of Lake Argyle, Northwestern Australia. *Environmental Management*, **29** (5): 634-646.

Figure captions

Figure 1. (a) Location of the Bléone catchment in France. (b) Location of the main local rivers, river monitoring stations, rain gauges and the town of Digne-les-Bains within the catchment. A dam is located at Malijai, at the catchment outlet.

Figure 2. Geology of the Bléone catchment. Location of the riverbed samples analysed in geochemistry and gamma spectrometry (n=30).

Figure 3. Contribution of the sediment yields measured in different sub-catchments to the total sediment exports from the Bléone catchment at Malijai during the (a) 2007-2009, (b) 2007-2008, (c) 2008-2009 periods. Reference is made to hydrological years (from October to September).

Figure 4. Dependence of Be-7 and Cs-137 concentrations on erosion processes in soil surface and riverbed samples collected in the Bléone catchment.

Figure 5. Contribution of each potential sediment source to each riverbed sediment sample (results from MM% model) collected during the four sampling campaigns: (a) 24 May 2007; (b) 8 January 2008; (c) 22 April 2009; (d) 18 May 2009.

Figure 6. (a) Relationship between EA% and MM% for the different geological substrate types. (b) Comparison between the *SSY* fraction per geologic type calculated based on the map of eroded areas (EA%) and on the results of the mixing model (MM%) applied to the riverbed samples collected close to the monitoring stations (except at Laval).

Figure 7. Distribution of erosion rates according to the sub-catchment and according to the geological substrate type over two different time scales: (a) mean inter-annual erosion rates (kg m^{-2} yr^{-1}) were estimated based on *SSY* measured during the entire 2007-2009 period; (b) erosion rates at the flood scale (t km^{-2} hr^{-1}) were estimated based on *SSY* measured during the major flood that occurred before the collection of riverbed sediment. No data were available for the Duyes station at the flood event scale. (c) Rainfall patterns observed during those floods and total erosion rates (t km^{-2} hr^{-1}) measured at each study site.

Fig. 1

(a)

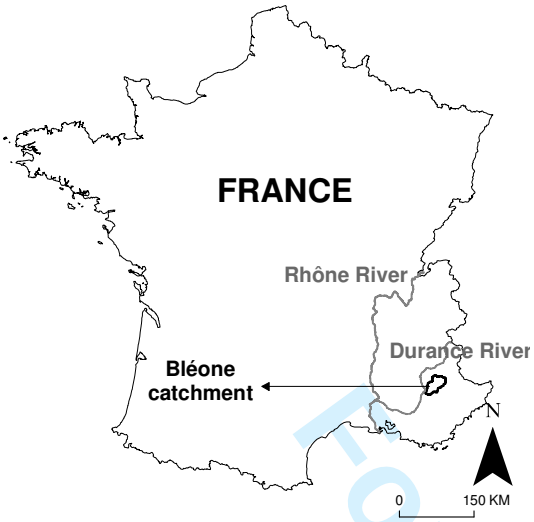

(b)

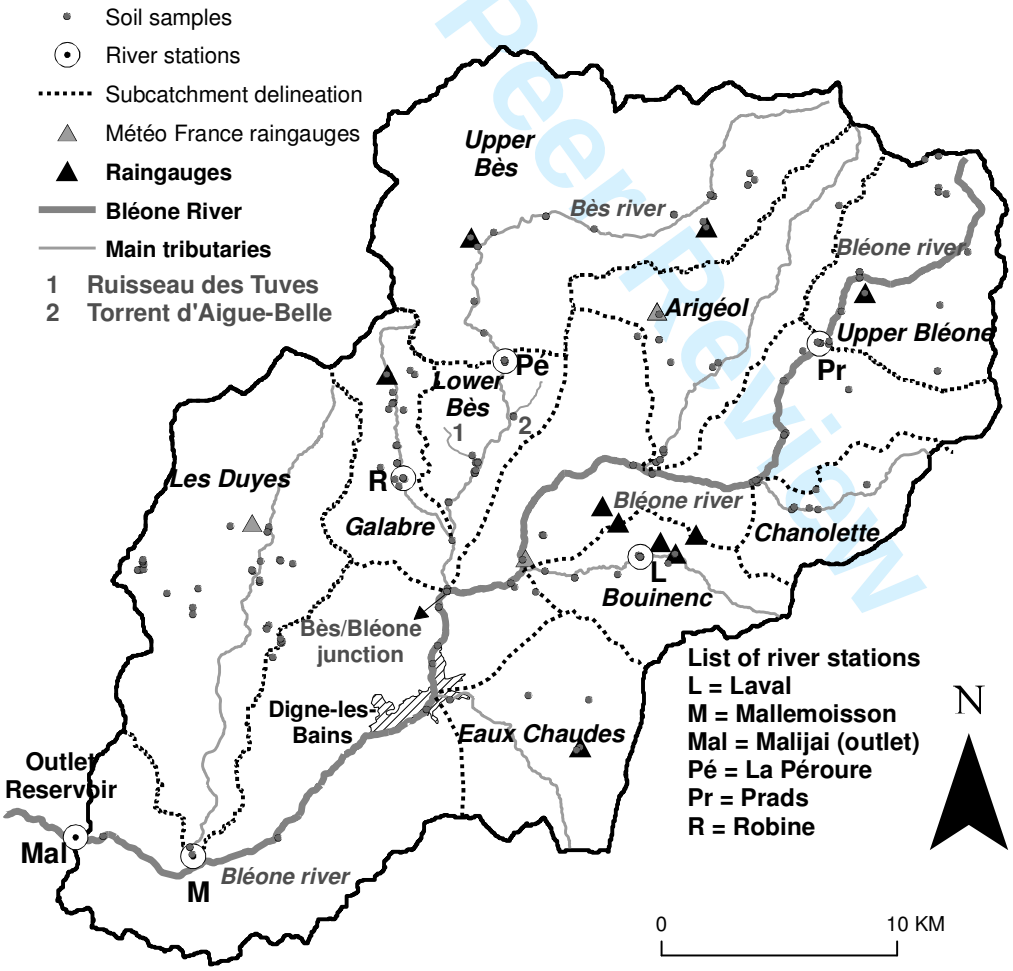

Figure 2.

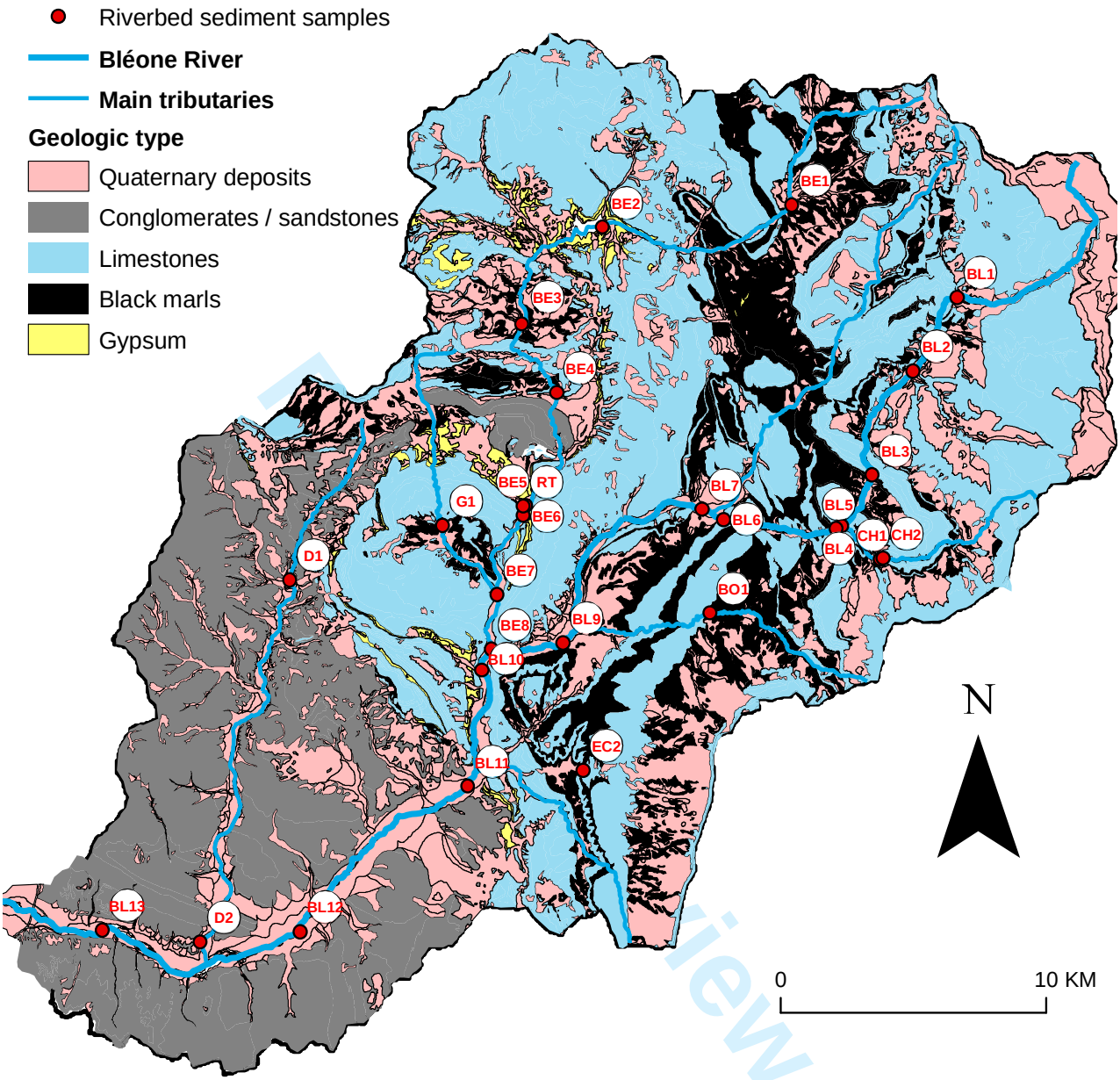
Riverbed sediment samples
Bléone River
Main tributaries
Geologic type
Quaternary deposits
Conglomerates / sandstones
Limestones
Black marls
Gypsum
BE1
BE2
BE3
BE4
BE5
RT
G1
BE6
D1
BE7
BE8
BL9
BL10
BL11
EC2
BL13
D2
BL12
BL1
BL2
BL3
BL7
BL6
BL5
BL4
CH1
CH2
BO1
N
0
10 KM

Fig. 3

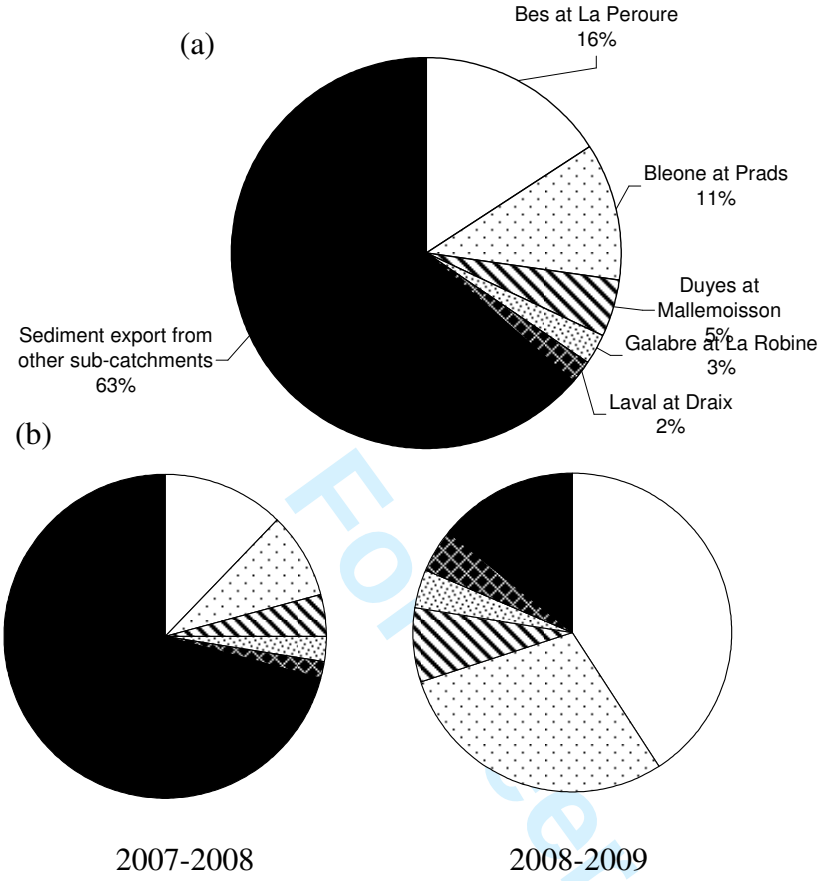

Fig. 4

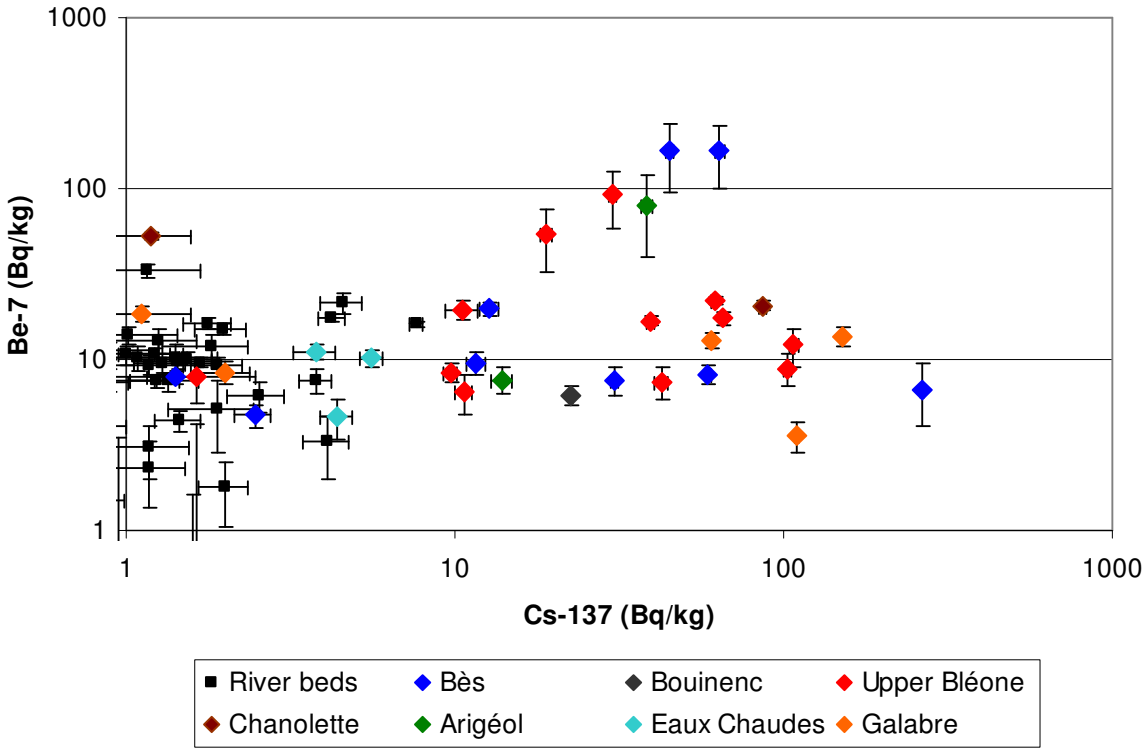

Fig. 5

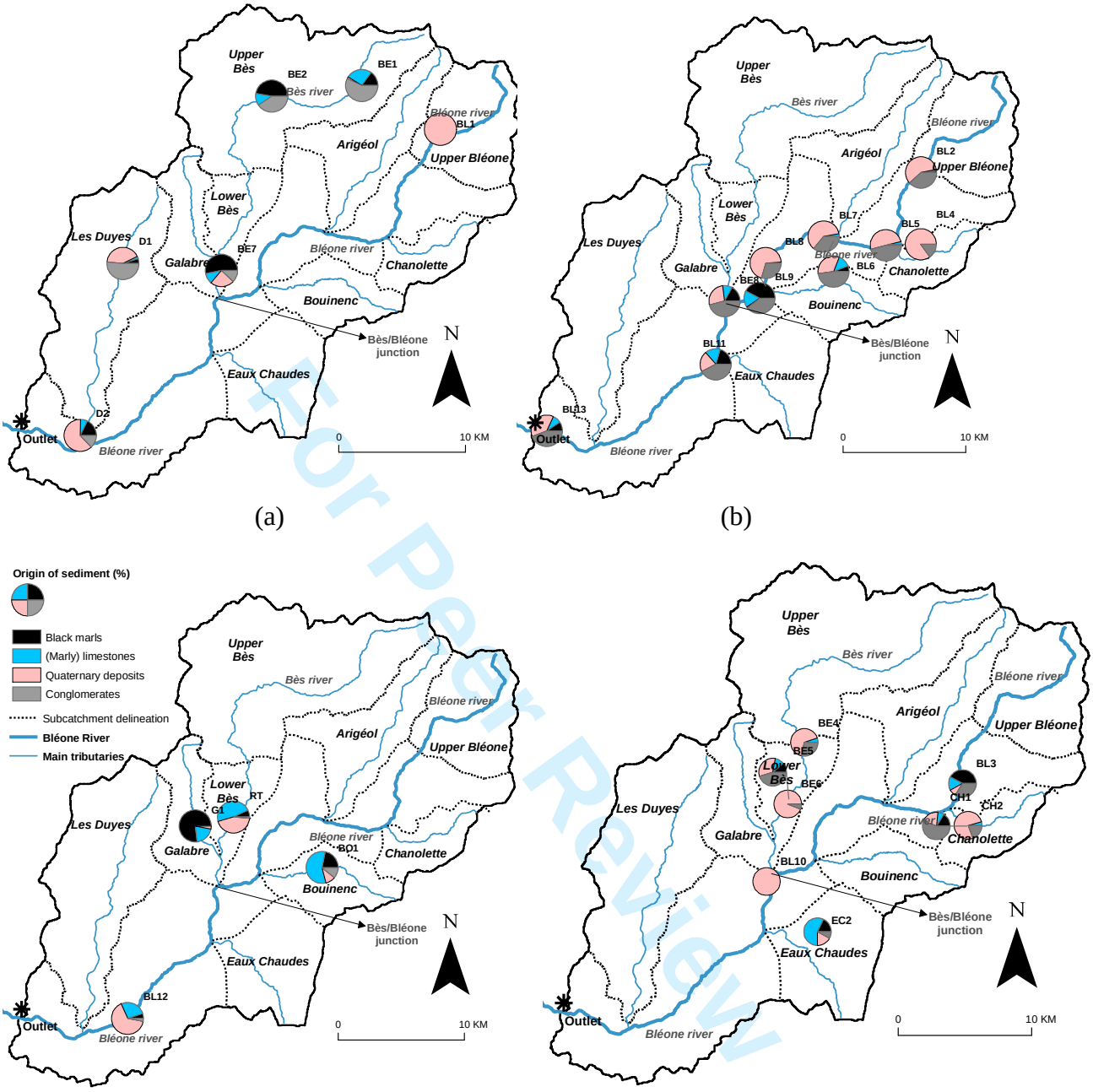

(a) (b) (c) (d)

Fig. 6

(a)

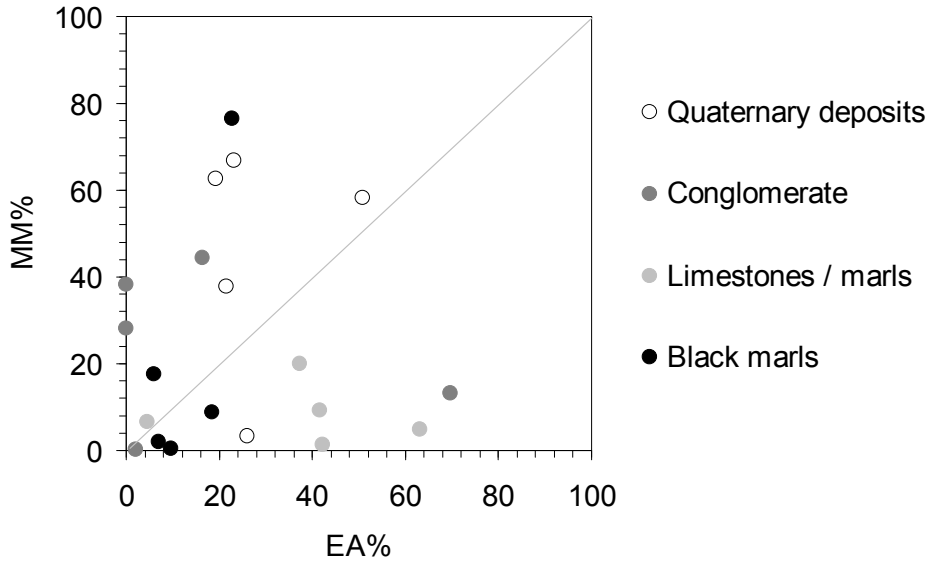

(b)

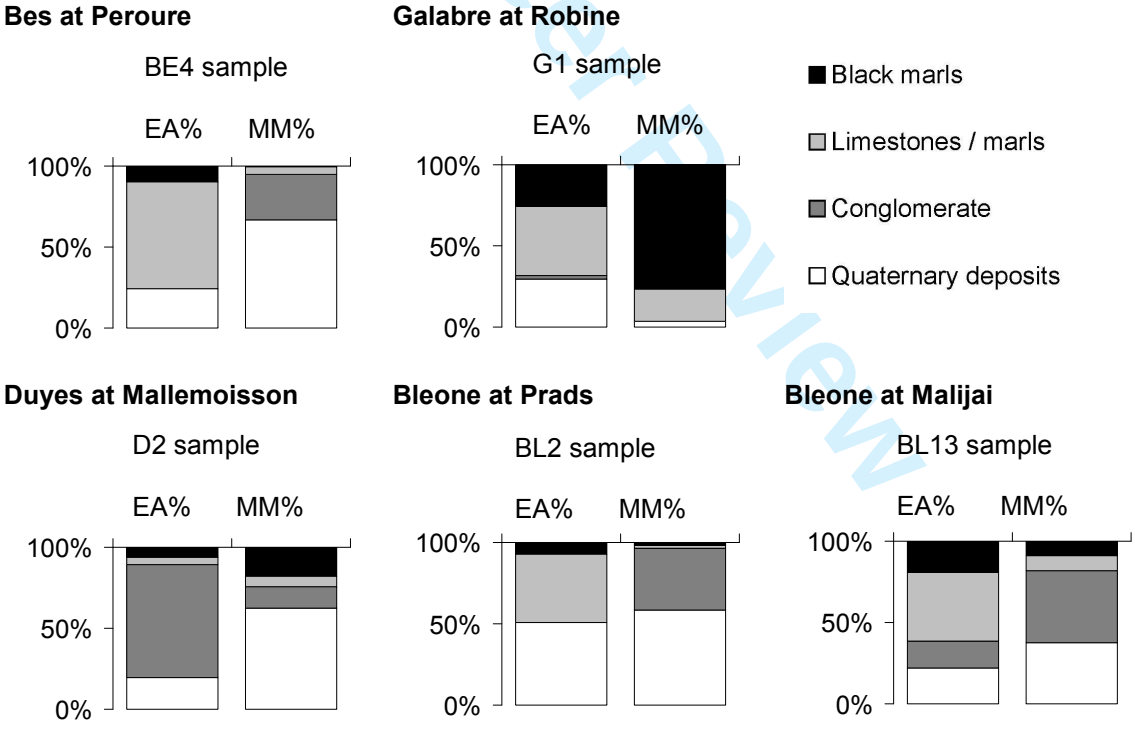

Fig. 7

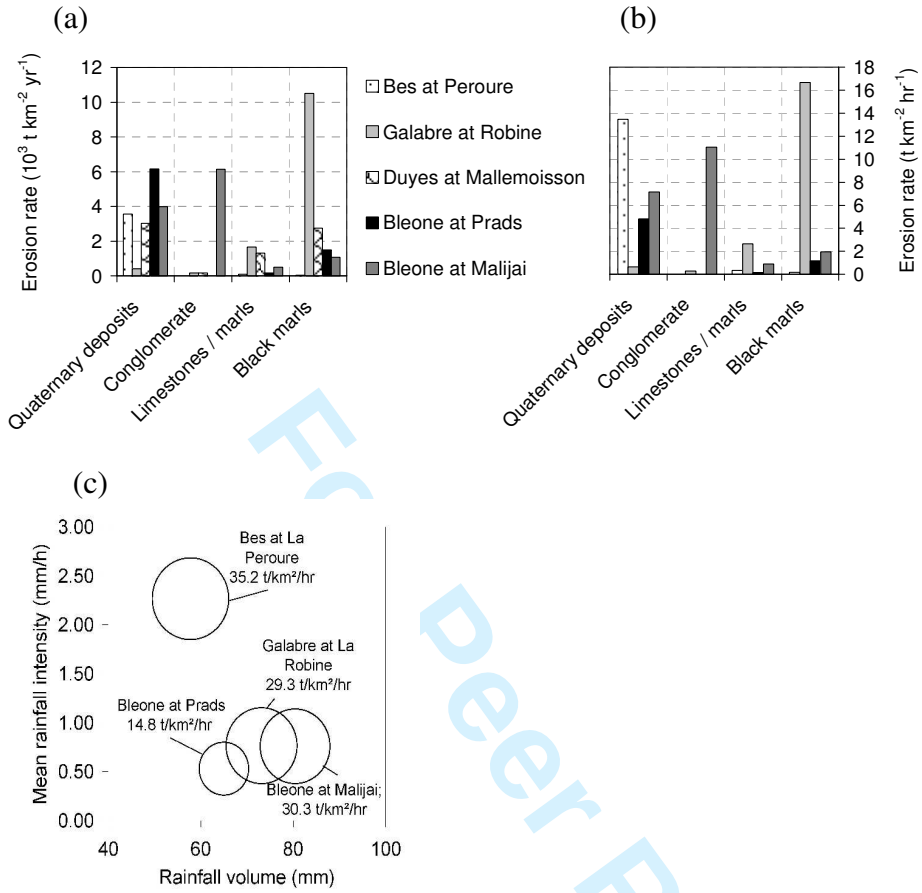

Table 1. Main characteristics of the river monitoring stations.

Station Number	River	Location	Drainage Area (km²)	Highly Eroded Area (%)	Geology (% area) [the remaining % correspond to Gypsum]				Land use (% area) [the remaining % correspond to urban areas]					Sampling frequency	
					Quaternary deposits	Conglomerate	Limestones / marls	Black marls	Forest	Cropland	Bare rocks	Sparse vegetation	Grassland	Water Level	Turbidity
1	Bléone	Malijai	870	11	27	25	37	10	43.6	5.0	6.9	30.7	13.1	Variable time-step	60 min.
2	Bès	Pérouré	165	17	20	15	51	12	42.6	1.9	15.7	18.2	21.4	Variable	10 min.
3	Bléone	Prads Haute-Bléone	65	7	37	15	46	2	24.2	0.0	33.9	33.9	6.3	10 min.	10 min.
4	Les Duyes	Mallemoisson	124	9	22	60	16	1	42.8	11.9	0.0	30.3	14.9	10 min.	10 min.
5	Galabre	La Robine	22	8	31	2	54	9	11.0	2.6	0.0	19.3	67.0	10 min.	10 min.
6	Laval	Draix	0.86	68	4	0	2	94	32	0.0	55.6	8.1	4.3	Variable	Variable

Table 2. Characteristics of collected river bed samples.

Sampling date	Samples	Last flood event	Spatial variability of rainfall : mean ± [min-max]	Rainfall type, snow cover
24/05/2007	BE1, BE2, BE7, BL1, D1, D2	02/05/2007 (1)	33 mm ± [23–50] (2)	No hail, no snow cover
08/01/2008	BE3, BE8, BL2, BL4 to BL9, BL11, BL13,	23/11/2007	80 mm ± [55–125] (2)	No hail, no snow cover
22/04/2009	BL12, BO1, G1, RT	15/04/2009	48 mm ± [30–68] (3)	No hail, no snow cover
18/05/2009	BE4, BE5, BE6, BL3, BL10, CH1, CH2, EC2	27/04/2009	20 mm ± [6–30] (3)	No hail, no snow cover

(1) Flood event observed on the Bléone river at Malijai; no data are available for the other stations before October 2007.
(2) Rainfall exclusively measured by four rain gauges (operated by *Météo France*) located in the Duyes, Upper Bès, Bléone and Upper Bléone catchments (Fig. 1b)
(3) Rainfall estimated based on the measurements of all rain gauges presented in Fig. 1b.

Table 3: Relevant discharge and sediment indicators derived from the monitoring of the river stations between 2007 and 2009.

Station Number	Station Name	Q_m (mm)	Q_{mx} ($m^3 s^{-1}$)	SSC_m (g L^{-1})	SSC_{mx} (g L^{-1})	SSF_m (t s^{-1})	SSF_{mx} (t s^{-1})	SSY (t)	SSY* (t km^{-2} yr^{-1})
1	Bleone at Malijai	410	138.8	0.3	99	0.0078	1.98	432 442	249
2	Bes at Pérouré	437	30.0	0.3	135	0.0011	0.60	68 921	209
3	Bleone at Prads	572	13.1	0.1	365	0.0008	2.53	49 001	377
4	Duyes at Mallemoisson	342	10.0	0.1	48	0.0004	0.22	20 261	85
5	Galabre at La Robine	287	5.5	0.4	131	0.0002	0.30	11 042	251
6	Laval at Draix	297	3.0	16.3	908	0.1500	0.72	8612	5007

Discharge parameters: Q_m (mean annual runoff depth); Q_{mx} (instantaneous peak flow discharge).

Sediment concentration parameters: SSC_m (mean sediment concentration); SSC_{mx} (peak sediment concentration).

Sediment flux and yield parameters: SSF_m (mean sediment flux); SSF_{mx} (peak sediment flux); SSY (total sediment yield); SSY^* (specific sediment yield).

Table 4. Mean radionuclide activities (± standard deviations) in different river bed and soil samples (in Bq kg^{-1}, except for K).

Type	n	Excess-Pb-210	Ra-226	Ra-228	K (%)	Cs-137	Be-7	Am-241
River beds	62	2.5 (± 6.6)	17.8 (± 4.9)	21.2(±5.5)	1.1 (± 0.5)	5.8 (± 25.8)	9.4 (± 7.0)	< 0.2
Sub-catchment soils (n=105)								
Upper Bléone	18	26.4 (± 28.0)	27.7 (± 8.8)	37.5 (± 13.6)	1.8 (± 0.8)	41.6 (± 46.3)	15.7 (± 22.9)	0.1 (± 0.4)
Bès	18	27.2 (± 29.6)	28.4 (± 9.2)	31.4 (± 9.3)	1.8 (± 1.0)	50.9 (± 59.7)	23.1 (± 52.2)	< 0.2
Galabre	20	8.7 (± 21.4)	26.0 (± 9.1)	27.4 (± 11.5)	1.8 (± 0.9)	36.6 (± 76.8)	3.2 (± 5.7)	< 0.2
Chanolette	2	33.0 (± 46.6)	20.5 (± 4.0)	28.1 (± 6.1)	1.4 (± 0.7)	43.9 (± 60.3)	36.7 (± 22.6)	< 0.2
Arigéol	8	30.9 (± 30.9)	20.6 (± 0.3)	26.6 (± 0.3)	1.4 (± 0.1)	54.6 (± 5.7)	10.8 (± 54.0)	0.2 (± 0.1)
Bouinenc	4	7.2 (± 6.7)	20.0 (± 4.1)	21.8 (± 1.5)	1.2 (± 0.1)	10.1 (± 11.5)	3.8 (± 2.6)	< 0.2
Eaux Chaudes	5	16.4 (± 21.6)	22.0 (± 2.7)	28.2 (± 7.1)	1.5 (± 0.2)	11.4 (± 17.8)	6.5 (± 4.5)	< 0.2
Les Duyes	30	21.4 (± 15.9)	19.0 (± 4.6)	25.1 (± 6.4)	1.1 (± 0.3)	41.5 (± 32.5)	n/a	< 0.2

n/a not analysed

Table 5. Mean activities in relevant radionuclides and mean concentrations in geochemical elements measured by INAA and ICP-MS in representative sediment sources.

(a) Relevant radionuclides (Bq kg^{-1})		Pb-210	Th-234	Ra-226	Ra-228	Th-228	K (%)	Cs-137
Black marl (Bathonian) -	mean	29.2	21.5	20.9	31.0	31.2	1.6	12.4
	SD	20.2	5.5	3.4	8.5	8.5	0.4	26.6
Other black marls-	mean	37.7	22.0	22.1	30.2	30.7	1.5	23.9
	SD	20.5	6.3	6.3	12.0	12.2	0.5	21.0
Grey marls-	mean	109.1	17.8	22.7	30.0	31.5	1.5	314.8
	SD	48.4	20.3	22.0	24.2	24.1	1.3	84.7
Marly limestones -	mean	42.8	34.8	42.7	24.3	24.4	1.7	24.2
	SD	3.7	2.3	2.1	1.8	0.3	0.8	2.3
Quaternary deposits -	mean	25.0	21.5	21.0	27.9	27.5	0.9	33.9
	SD	2.5	1.9	1.1	0.8	1.3	0.0	44.5
Conglomerates -	mean	44.0	18.9	18.2	29.3	28.9	1.2	35.0
	SD	22.5	1.3	0.4	2.8	1.6	0.1	24.9
Gypsum -	mean	26.4	22.5	22.0	21.6	21.6	1.3	6.9
	SD	10.3	18.8	13.9	23.5	23.1	0.4	3.3

(b) Major elements (%)		K	Na	Fe	Mg	Al	Ca	Ti
Black marl (Bathonian) -	mean	1.9	0.3	3.0	0.8	5.9	17.4	0.3
	SD	0.4	0.0	0.7	0.2	1.4	9.0	0.0
Other black marls -	mean	1.7	0.4	2.7	0.8	5.9	14.6	0.3
	SD	0.6	0.1	0.6	0.2	1.6	9.0	0.1
Grey marls -	mean	1.6	1.0	2.7	0.7	6.0	6.3	0.4
	SD	1.5	0.5	2.7	3.3	4.1	16.9	0.2
Marly limestones -	mean	1.9	0.1	2.0	2.2	4.0	10.2	0.2
	SD	1.7	0.0	0.9	2.4	0.3	6.9	0.0
Quaternary deposits -	mean	1.1	0.2	1.6	0.6	2.2	25.0	0.2
	SD	0.1	0.1	0.0	0.0	0.2	1.1	0.0
Conglomerates -	mean	1.3	0.1	2.5	0.5	4.3	11.4	0.2
	SD	0.0	0.0	0.1	0.1	0.1	3.0	0.0
Gypsum -	mean	1.4	1.7	3.8	0.8	3.8	11.2	0.2
	SD	0.4	1.6	0.6	0.3	4.2	11.9	0.2

(c) Trace elements (mg kg^{-1})		As	Ba	Ce	Co	Cr	Eu	Fe	Hf	K	La	Lu	Na	Th	Rb	Sb
Black marls (Bathonian) -	mean	7.0	179.6	69.8	15.8	66.4	0.9	3.0	2.8	1.9	46.2	0.3	0.3	7.6	142.2	0.9
	SD	3.0	16.1	22.2	4.1	32.8	0.4	0.7	0.7	0.4	32.1	0.0	0.0	1.8	68.3	0.2
Grey marls -	mean	6.0	259.0	67.0	14.0	93.0	0.7	2.7	4.7	1.6	28.0	0.4	1.0	8.0	116.0	0.8
	SD	9.1	169.0	48.8	12.8	64.8	0.6	2.7	2.5	1.5	25.8	0.3	0.5	6.0	84.5	0.8
Quaternary deposits -	mean	7.3	122.8	45.5	5.0	40.0	0.6	1.6	5.3	1.1	21.5	0.2	0.2	7.5	51.5	0.5
	SD	0.8	16.6	2.1	0.0	4.2	0.1	0.0	0.3	0.1	0.7	0.0	0.1	0.7	9.2	0.1
Conglomerates -	mean	7.1	221.6	45.0	11.0	67.5	0.8	2.5	3.4	1.3	25.5	0.4	0.1	7.0	86.5	1.4
	SD	1.9	0.1	11.3	0.0	31.8	0.0	0.1	0.1	0.0	3.5	0.1	0.0	0.0	10.6	0.0
Other black marls -	mean	6.8	240.0	56.3	10.7	65.3	0.8	2.7	2.4	1.7	30.7	0.3	0.4	6.7	98.7	1.0
	SD	2.5	95.2	20.5	3.1	16.9	0.2	0.6	0.8	0.6	11.2	0.1	0.1	2.5	34.4	0.4
Marly limestones -	mean	5.6	173.5	41.5	8.0	42.5	0.6	2.0	1.9	1.9	23.7	0.2	0.1	5.5	95.5	1.0
	SD	4.2	50.2	16.3	4.2	6.4	0.1	0.9	0.9	1.7	8.9	0.1	0.0	2.1	46.0	0.2
Gypsum -	mean	6.3	207.5	77.2	9.5	115.1	0.4	3.8	3.3	1.4	25.0	0.1	1.7	7.4	72.0	0.6
	SD	0.7	130.8	10.2	10.6	39.7	0.5	0.6	2.3	0.4	17.7	0.2	1.6	3.7	101.8	0.7

		Sc	Sm	Zn	V	Mn	Ni	Cu	Ag	Cd	Tl	Pb
Black marls (Bathonian) -	mean	12.2	6.4	82.4	103.4	1004.6	47.6	17.5	0.2	0.1	0.6	28.2
	SD	2.3	2.3	12.4	9.6	303.9	7.3	2.8	0.1	0.0	0.1	13.4
Limy marls -	mean	11.0	4.4	102.0	73.0	310.0	42.0	11.0	0.1	0.1	0.4	16.7
	SD	8.9	3.8	78.3	77.6	644.1	42.3	15.4	0.2	0.2	0.4	17.3
Quaternary deposits -	mean	5.4	3.6	44.0	43.7	200.2	17.3	7.2	0.1	0.1	0.3	9.8
	SD	0.3	0.1	15.6	3.0	1.9	1.6	1.2	0.0	0.0	0.0	1.4
Conglomerates -	mean	8.4	4.7	87.5	56.0	707.1	44.7	20.2	0.2	0.3	0.5	23.1
	SD	0.4	0.6	16.3	8.2	158.6	10.7	1.8	0.1	0.0	0.1	6.1
Other black marls -	mean	11.1	5.0	86.0	74.2	560.3	39.3	17.2	0.2	0.1	0.5	113.4
	SD	3.8	1.6	34.4	21.2	119.3	9.3	6.4	0.0	0.1	0.2	170.3
Marly limestones -	mean	7.6	3.7	41.5	52.9	385.5	36.7	12.0	0.1	0.2	0.5	12.3
	SD	2.8	1.1	10.6	5.9	19.3	17.2	6.4	0.1	0.1	0.2	4.9
Gypsum -	mean	13.6	4.9	44.5	58.7	336.0	36.8	11.1	0.1	0.1	0.4	12.3
	SD	2.7	0.7	62.9	72.0	387.3	43.2	7.8	0.1	0.1	0.4	10.3

SD : Standard Deviation

To facilitate their analysis and interpretation, the seven rock types were regrouped into five classes (black marls of Bathonian age and other black marls were regrouped in one class; grey marls and marly limestones were regrouped in one class, entitled “limestones”).

Table 6. Mean activities in relevant radionuclides and mean concentrations in geochemical elements measured by INAA and ICP-MS in riverbed sediment collected along the river network (BE: Bès river; BL: Bléone river; BO: Bouinenc river; CH: Chanolette river; D: Duyes river; EC: Eaux Chaudes river; G: Galabre river; RT: Ruisseau des Tuves).

(a) Relevant radionuclides (Bq kg^{-1})	Pb-210	Th-234	Ra-226	Ra-228	Th-228	K (%)	Cs-137
BE01	15.7	13.7	14.9	21.6	22.3	1.0	1.1
BE02	20.8	14.5	15.1	22.8	22.8	1.0	1.6
BE04	18.3	18.9	18.1	17.6	18.2	1.0	1.3
BE05	23.6	20.4	19.8	24.2	24.1	1.2	1.8
BE06	12.4	18.8	16.7	14.4	13.9	1.0	0.9
BE07	21.4	22.4	21.7	23.6	23.4	1.9	4.6
BE08	22.3	16.2	20.1	23.3	23.7	1.2	2.5
BL01	10.6	9.0	8.8	9.9	9.6	0.5	3.8
BL02	26.8	14.3	15.1	17.5	17.5	0.8	7.7
BL03	16.0	15.6	15.9	20.6	20.7	1.0	1.1
BL04	10.2	8.7	9.6	10.5	10.6	0.6	1.9
BL05	16.9	16.4	15.7	19.4	20.6	0.7	1.2
BL06	26.9	16.6	16.2	20.6	21.0	0.8	4.2
BL07	10.8	9.8	12.9	15.8	15.6	0.6	1.0
BL08	23.4	17.5	16.1	19.9	20.6	0.8	4.1
BL09	15.9	16.6	17.6	25.2	24.5	1.1	0.9
BL10	11.4	10.3	11.4	11.0	10.2	0.6	1.3
BL11	15.1	13.2	17.5	20.8	21.6	1.0	1.0
BL12	16.9	15.4	17.3	20.0	20.2	0.9	1.6
BL13	19.2	15.3	17.1	20.6	20.5	1.0	1.5
BO1	15.5	16.2	21.2	26.8	26.5	1.1	0.0
CH01	15.0	14.9	17.7	23.6	22.8	0.9	1.8
CH02	14.9	12.8	16.4	18.0	18.3	0.7	1.2
D01	15.8	17.5	16.9	22.5	22.5	1.1	1.2
D02	17.0	12.8	14.1	17.9	18.2	1.0	1.9
EC2	21.5	15.3	18.4	26.2	26.3	1.1	0.3
G1	65.9	24.4	26.7	33.5	33.2	1.6	166.7
RT	34.9	26.6	34.8	26.1	26.5	3.4	0.9

(b) Major elements (%)	K	Na	Fe	Mg	Al	Ca	Ti
BE01	1.1	0.3	4.9	0.7	4.3	15.1	0.2
BE02	1.2	0.4	3.7	0.8	5.0	14.5	0.3
BE04	1.0	0.2	3.2	1.0	2.9	25.5	0.2
BE05	1.2	0.3	2.9	0.9	3.7	18.2	0.3
BE06	1.1	0.2	2.3	1.1	2.3	25.8	0.1
BE07	2.1	0.2	2.5	2.0	4.7	15.2	0.3
BE08	1.3	0.3	2.5	1.1	4.0	18.5	0.3
BL01	0.8	0.2	1.2	0.3	2.0	26.1	0.1
BL02	0.9	0.3	1.7	0.6	3.1	20.8	0.2
BL03	1.4	0.2	2.2	0.6	4.7	19.2	0.3
BL04	0.6	0.3	1.7	0.6	2.6	23.8	0.1
BL05	0.7	0.2	2.5	0.7	3.2	21.2	0.2
BL06	0.8	0.3	2.3	0.7	3.6	18.4	0.2
BL07	0.7	0.2	1.9	0.7	3.0	22.9	0.2
BL08	0.8	0.3	2.0	0.6	2.9	22.1	0.2
BL09	1.4	0.4	3.6	1.2	4.8	14.7	0.3
BL10	0.6	0.2	1.8	0.6	1.7	28.4	0.1
BL11	1.6	0.3	2.9	1.2	4.1	16.7	0.3
BL12	0.2	0.0	0.4	0.6	2.8	30.1	0.2
BL13	1.1	0.3	2.4	1.1	3.6	17.9	0.2
BO1	1.3	0.3	5.6	0.7	4.1	23.0	0.3
CH01	0.9	0.1	2.6	0.5	4.1	21.8	0.2
CH02	0.8	0.1	3.1	0.4	2.7	25.9	0.1
D01	1.0	0.5	2.1	0.9	3.5	14.4	0.2
D02	0.9	0.4	1.6	1.0	3.3	16.8	0.2
EC2	1.4	0.3	4.2	0.7	3.9	24.5	0.3
G1	2.0	1.1	3.1	0.7	5.3	8.3	0.5
RT	3.9	0.2	1.9	2.0	3.3	22.2	0.2

(c) Trace elements (mg kg^{-1})	As	Ba	Ce	Co	Cr	Eu	Fe	Hf	K	La	Lu	Na	Th	Rb	Sb
BE01	30.1	184.0	46.5	28.5	56.1	0.9	4.9	2.2	1.1	22.8	0.3	0.3	5.9	66.0	0.8
BE02	14.1	212.0	47.1	17.5	59.7	0.8	3.7	2.5	1.2	23.0	0.3	0.4	6.1	71.0	0.8
BE04	15.8	129	11	15	36	0.7	3.2	1.7	1.0	18	0.3	0.2	4	51	0.6
BE05	9.9	190	43	12	50	0.7	2.9	2.8	1.2	23	0.2	0.3	5	60	0.6
BE06	12.0	195	33	11	30	0.7	2.3	1.8	1.1	16	0.2	0.2	3	34	0.6
BE07	5.6	208	47.9	10.4	48.8	0.7	2.5	2.7	2.1	21.7	0.2	0.2	6.2	60.2	0.4
BE08	8.4	189.0	42.0	11.2	50.3	0.7	2.5	2.6	1.3	21.7	0.3	0.3	6.0	54.2	0.6
BL01	3.1	321.0	19.5	5.8	22.8	0.3	1.2	0.8	0.8	12.0	0.1	0.2	2.9	49.4	0.5
BL02	3.8	483	29.4	7.3	45.7	0.6	1.7	1.7	0.9	18.5	0.2	0.3	5.0	45.3	0.1
BL03	7.8	516	49	12	59	0.8	2.2	2.1	1.4	27	0.2	0.2	7	78	0.6
BL04	4.5	362	24.9	7.5	40.6	0.5	1.7	1.9	0.6	14.5	0.2	0.3	3.4	50.6	0.1
BL05	5.5	948	34.3	9.0	46.8	0.7	2.5	1.9	0.7	19.5	0.2	0.2	5.4	47.1	0.3
BL06	6.0	553	43.4	9.6	55.7	0.6	2.3	2.5	0.8	21.5	0.3	0.3	5.9	56.4	0.2
BL07	3.4	469	33.3	7.6	44.3	0.6	1.9	1.5	0.7	17.3	0.3	0.2	4.0	37.1	0.2
BL08	4.4	504	35.6	8.8	47.9	0.6	2.0	1.9	0.8	17.8	0.2	0.3	4.6	58.4	0.2
BL09	10.7	198	59.1	16.7	69.9	0.7	3.6	2.7	1.4	26.4	0.3	0.4	6.9	64.1	0.2
BL10	6.5	154	26	9	22	0.6	1.8	0.9	0.6	13	0.1	0.2	3	0	0.5
BL11	8.3	211	32.9	13.3	69.5	0.8	2.9	2.1	1.6	24.1	0.2	0.3	6.0	71.5	0.2
BL12	1.2	305	5	2	9	0.0	0.4	0.0	0.2	3	0.0	0.0	1	0	0.4
BL13	7.7	221	43.7	10.5	54.2	0.7	2.4	2.6	1.1	21.0	0.3	0.3	5.1	50.5	0.1
BO1	29.9	305	52	29	72	0.7	5.6	3.0	1.3	27	0.3	0.3	7	83	0.9
CH01	6.8	486	36	10	44	0.7	2.6	2.0	0.9	20	0.2	0.1	6	39	0.5
CH02	8.3	1344	35	11	34	0.7	3.1	1.5	0.8	19	0.2	0.1	5	0	0.4
D01	7.9	228.0	39.3	8.7	57.6	0.6	2.1	3.2	1.0	18.1	0.2	0.5	4.7	51.4	0.6
D02	3.9	179	45.9	6.8	59.8	0.6	1.6	2.5	0.9	21.4	0.2	0.4	5.2	59.7	0.3
EC2	20.4	409	58	23	59	0.8	4.2	2.6	1.4	26	0.3	0.3	6	71	0.7
G1	6.2	274	67	13	103	0.9	3.1	4.6	2.0	32	0.3	1.1	8	88	0.7
RT	9.0	594	49	10	39	0.6	1.9	2.4	3.9	21	0.2	0.2	6	49	0.6

	Sc	Sm	Zn	V	Mn	Ni	Cu	Ag	Cd	Tl	Pb
BE01	10.2	4.3	156.5	73	1168	58	35	0.17	0.13	0.32	22.1
BE02	10.1	4.0	119.9	81	1128	59	33	0.15	0.12	0.38	18.1
BE04	7.2	3.3	87	45	885	35	20	0.12	0.12	0.28	13.1
BE05	8.1	3.6	80	58	587	34	18	0.08	0.14	0.33	12.9
BE06	5.7	2.9	47	36	620	27	12	0.07	0.29	0.22	9.7
BE07	8.4	3.7	63.5	69.0	502.0	31.0	17.0	0.1	0.1	0.3	12.1
BE08	8.2	3.7	57.5	59	615	34	19	0.06	0.13	0.32	12.2
BL01	3.7	2.0	48.0	30	304	25	29	0.34	0.15	0.21	10.4
BL02	5.9	3.1	71.5	48.0	313.0	27.0	22.0	0.2	0.2	0.3	13.2
BL03	9.4	4.1	96	77	333	34	35	0.17	0.15	0.44	12.6
BL04	4.8	2.4	88.3	37.0	341.0	23.0	23.0	0.2	0.2	0.2	10.4
BL05	6.8	3.5	129.1	50.0	377.0	31.0	35.0	0.4	0.2	0.3	12.3
BL06	7.7	3.6	97.0	59.0	406.0	33.0	31.0	0.3	0.2	0.3	13.0
BL07	6.9	3.2	89.5	48.0	531.0	30.0	30.0	0.8	0.1	0.2	18.6
BL08	6.7	3.2	82.7	45.0	454.0	27.0	24.0	0.3	0.1	0.2	11.0
BL09	11.4	4.0	101.0	79.0	857.0	47.0	25.0	0.2	0.1	0.4	17.4
BL10	4.8	3.1	40	25	538	20	11	0.05	0.11	0.14	7.0
BL11	9.6	3.9	96.4	66.0	695.0	37.0	20.0	0.3	0.1	0.3	13.9
BL12	1.0	0.4	0	68	732	42	24	0.18	0.14	0.28	16.4
BL13	7.9	3.7	76.9	57.0	624.0	33.0	19.0	0.2	0.1	0.3	13.8
BO1	11.8	4.8	105	97	1083	78	34	0.31	0.13	0.44	33.1
CH01	7.4	3.1	80	59	352	33	27	0.22	0.13	0.34	13.5
CH02	6.5	3.7	81	43	413	36	32	0.43	0.14	0.32	12.7
D01	5.6	3.5	67.9	48	529	33	16	0.07	0.12	0.34	12.4
D02	5.6	3.4	58.5	57.0	539.0	27.0	10.0	0.1	0.1	0.3	10.0
EC2	11.5	4.0	125	90	1548	64	33	0.17	0.14	0.40	25.0
G1	12.5	5.0	93	115	349	50	15	0.12	0.14	0.40	15.2
RT	7.9	3.4	0	53	471	25	13	0.07	0.07	0.36	10.0

Table 7. Results of the Kruskal-Wallis *H*-test applied to the potential fingerprint properties measured in the sediment sources collected in the Bléone catchment.

Potential fingerprint	H-value
Parameters measured by gamma spectrometry	
Cs-137	4.35
K-40	5.94
Pb-210	5.55
Ra-226	6.58 (*)
Ra-228	3.20
Th-234	5.66
Th-228	2.62
Parameters measured by INAA	
As	1.86
Ba	6.15 (*)
Ce	5.46
Co	9.64 (*)
Cr	5.63
Eu	8.51 (*)
Fe	7.28 (*)
Hf	7.87 (*)
K	5.67
La	6.13 (*)
Lu	10.82 (*)
Na	8.47 (*)
Pa (Th)	2.98
Rb	6.68 (*)
Sb	8.73 (*)
Sm	6.17 (*)
Zn	6.67 (*)
Parameters measured by ICP-MS	
Ag	7.32 (*)
Al	11.58 (*)
Ca	2.86
Cd	5.75
Cu	7.05 (*)
Mg	5.92
Mn	10.22 (*)
Ni	6.39 (*)
Ti	7.83 (*)
Pb	5.91
Tl	9.13 (*)
V	14.29 (*)

(*) Difference significant at p=0.05.

Table 8. Results of the stepwise discriminant function analysis to identify the optimum composite fingerprint.

Fingerprint property added	Wilk's lambda	Cumulative % of samples classified correctly
Ra-226	0.040483	70.6
Al	0.007641	83.4
Ni	0.002403	89.9
V	0.000103	93.9
Cu	0.000515	96.9
Ag	0.000253	100

Table 9. Erosion rates (mm yr^{-1}) of each rock type during the 2007-2009 period. Rates were estimated using a compacted sediment density of 2,650 kg m^{-3}.

River monitoring station	Erosion rate (mm yr^{-1})			
	Quaternary deposits	Conglomerate	Limestones / marls	Black marls
Bès at Peroure	1.34	0.00	0.03	0.02
Galabre at Robine	0.15	0.07	0.63	3.97
Duyes at Mallemoisson	1.14	0.07	0.50	1.03
Bleone at Prads	2.32	---	0.07	0.57
Bleone at Malijai	1.50	2.32	0.19	0.41
Laval at Draix	---	---	---	2.92